Materials Horizons

ROYAL SOCIETY OF CHEMISTRY

REVIEW

View Article Online
View Journal

Cite this: DOI: 10.1039/d5mh00676g

Research on light-responsive luminescence properties of carbon dots and their applications

Zhimeng Ma, Qiang Fu, * Kailin Zhang, Shouhong Sun and Mingbo Yue

Received 11th April 2025,
Accepted 7th May 2025

DOI: 10.1039/d5mh00676g

rsc.li/materials-horizons

Carbon dots (CDs), as zero-dimensional carbon-based nanomaterials, have become a new generation of smart luminescent materials because of their tunable optical properties, excellent biocompatibility and controllable synthesis strategies. On the basis of the difference in their optical response behavior, CDs can be classified into two main systems: photoluminescent and photochromism. Photoluminescent CDs achieve luminescence, including fluorescence, room temperature phosphorescence (RTP), and thermally activated delayed fluorescence (TADF), through the modulation of the carbon core structure, surface state engineering, molecular state jumping, and crosslink-enhanced emission (CEE) mechanisms. On the other hand, photochromic CDs confer dynamic optical response properties to materials through free radical-mediated electron transfer, energy transfer modulation, or molecular isomerization. In this review, we systematically elucidate the underlying luminescence mechanisms of these two types of systems and introduce the unique properties and application prospects of photoresponsive CDs in biomedicine, catalysis, and anticounterfeiting. We summarize the latest research progress on photoresponsive CDs, analyze their material properties, and discuss the key challenges to be addressed in their future development.

Wider impact

Carbon dots (CDs), as versatile and tunable luminescent nanomaterials, hold significant potential for advancing multiple fields due to their unique photoresponsive properties. Their applications in biomedicine—such as bioimaging, drug delivery, and diagnostics—could lead to safer, more efficient theranostic platforms with enhanced biocompatibility. In catalysis, CDs may enable more sustainable and energy-efficient processes, contributing to green chemistry initiatives. Additionally, their dynamic optical properties offer innovative solutions for high-security anticounterfeiting technologies, benefiting industries ranging from pharmaceuticals to luxury goods. However, the widespread adoption of photoresponsive CDs requires addressing key challenges, including scalability, long-term stability, and precise control over their optical behaviors. By overcoming these hurdles, CDs could revolutionize smart materials, fostering interdisciplinary innovations that bridge nanotechnology, biotechnology, and environmental science. This review not only consolidates current knowledge but also highlights pathways for future research to unlock the full societal and industrial potential of these emerging nanomaterials.

College of Engineering, Qufu Normal University, Rizhao, Shandong 276826, People's Republic of China. E-mail: qiang.fu@qfnu.edu.cn

Zhimeng Ma

ZhiMeng Ma received his bachelor's degree from the School of Automation at Zhengzhou University of Industrial Technology in 2023. He is currently pursuing a Master's degree at Qufu Normal University. His research interests are focused on the luminescence properties of carbon dot-based composite materials.

Qiang Fu

Qiang Fu, currently serving as the master tutor at Qufu Normal University, earned his PhD from Beijing Normal University in 2020. His primary research team specializes in optical material design, fundamental mass spectrometry techniques, and the electrochemical synthesis of nanomaterials.

1. Introduction

The luminescence properties of materials have great potential for use in biomedicine, fluorescence sensing, and photoelectrocatalysis.[1,2] However, real-world implementation requires not only enhanced luminescence but also material safety, stability, and design flexibility considerations. For instance, biomedical applications demand materials with high fluorescence brightness and low cytotoxicity, whereas environmental sensors necessitate selective responsiveness to target pollutants. Traditional luminescent media such as cadmium-containing quantum dots or organic dyes suffer from toxicity, photobleaching, and exorbitant synthesis costs, limiting their widespread application. In light of these findings, CDs, zero-dimensional carbon-based nanomaterials typically less than 10 nm in size, were discovered inadvertently *via* the purification of single-walled carbon nanotubes in 2004 and since then have been novel alternatives.[3] Due to their unique photoresponsive properties, high biocompatibility, ecological sustainability, and low-cost manufacturing, CDs represent promising replacements for traditional materials. The CDs family includes graphene quantum dots (GQDs), carbon quantum dots (CQDs), carbon nanodots (CNDs), and carbon polymer dots (CPDs).[4,5] Compared with heavy metal quantum dots and organic dyes, CDs not only avoid these issues, such as heavy metal toxicity and low photostability but also have the advantages of tunable emission wavelengths, high fluorescence quantum yields (QYs), and RTP. Over nearly two decades of research, advancements in synthesis and functionalization have expanded their applications to optoelectronics, bioimaging, environmental monitoring, antibacterial therapies, and dynamic encryption, thereby establishing themselves as utilitarian and multifunctional nanomaterials.[6–8]

The optical properties of CDs are intricately linked to their surface functional groups, carbon core composition, and size distribution, enabling light-responsive behaviors. Photoresponsive CDs can exhibit diverse luminescence behaviors under light conditions and can be classified into two major systems, namely, photoluminescent and photochromic systems, on the basis of their post-illumination properties.[9] Photoluminescent CDs include fluorescence,[10,11] RTP,[12,13] and TADF.[14,15] Reports in the literature indicate that the luminescence mechanisms of CDs may involve surface state emission, CEE, quantum size effects, and carbon core-dominated emission.[16–23] By regulating these mechanisms, researchers have made a series of breakthroughs. For example, in 2021, Qu *et al.*[24] developed time-dependent phosphorescence color (TDPC) materials based on CDs by precisely modulating their surface states and carbon core configurations. Subsequent studies by Li *et al.*[25] demonstrated that minor Mn doping in zeolitic frameworks subtly altered the microenvironment of the embedded CDs. This environmental modulation significantly influences the surface state, leading to the formation of distinct exciton species. Under UV irradiation at 298 K, the system exhibited a dynamic afterglow transition from red to green, whereas at 77 K, time-resolved phosphorescence evolved from green to cyan and finally blue. These phenomena collectively enable temperature-dependent TDPC regulation. Yang *et al.*[26] revealed that the 510 nm emission of citric acid (CA)-ethylenediamine-derived CPDs originating from molecular fluorophores evolved *via* quantum confinement effects. The photoluminescence mechanism involves the synergistic evolution of multiple fluorophores. By isolating a novel molecular fluorophore, IATO, from CA–ethylenediamine CPDs, they confirmed its derivation from IPCA through quantum confinement-driven structural evolution. This discovery, corroborated in other systems, establishes a universal strategy for tailoring CPDs' optical properties. In contrast,

Kailin Zhang

Kailin Zhang received his BS degree from the College of Engineering at Qufu Normal University in 2022. He is currently pursuing a master's degree at Qufu Normal University. His research interests are primarily focused on the synthesis and application of photochromic carbon dots.

Shouhong Sun

Shouhong Sun received her BS degree from the College of Engineering (2022), Qufu Normal University, China. Currently, she is studying for her MS degree at the College of Engineering, Qufu Normal University. Her research interests are mainly focused on the synthesis and application of carbon dot-based afterglow materials.

Mingbo Yue

Mingbo Yue, currently serving as a professor at Qufu Normal University, earned his PhD from Nanjing University in 2007. His research is focused on functionalized nanoporous materials for catalysis and adsorption applications.

photochromic CDs exhibit dynamic, reversible optical changes under light irradiation, driven by mechanisms such as free radical-mediated electron transfer, energy transfer modulation, and molecular isomerization. For example, spiropyran (SP)-functionalized CDs undergo reversible ring-opening isomerization under UV light, converting them into merocyanine (MC) with distinct absorption and emission spectra.[27–29] Further advancing this field, Wu *et al.*[30] engineered ternary supramolecular nanoparticles by integrating CDs as anions into cationic nanofibers composed of a dithienylethene derivative (functionalized with styrylpyridinium groups) and cucurbit[8]uril (CB[8]). This assembly achieved light-triggered multicolor luminescence (gold, yellow, khaki, and blue) and reversible white-light emission through UV/vis irradiation, showing programmable fluorescence switching for optical encoding. Similarly, Chen *et al.*[31] developed a hydrothermal strategy to embed naphthalimide (NI) moieties into CDs, followed by polyvinylpyrrolidone coating, yielding a multifunctional material with dual photochromism and long-lived afterglow. Upon irradiation, the material transitioned from colorless to brown in appearance and from blue to yellow in emission, which was attributed to the *in situ* generation of NI radical anions. These anions not only enabled intrinsic photochromism but also facilitated stimuli-responsive afterglow behavior, including humidity- and oxygen-dependent luminescence switching. These studies provide critical insights into light-responsive mechanisms, guiding the design of advanced luminescent materials (Fig. 1).

The synthesis of CDs plays a crucial role in determining their optical properties and functionalities. Typically, their formation occurs in two stages. Initially, precursors and solvents undergo oxidation and dehydration reactions at specific temperatures, forming nucleation centers. As carbonization progresses, these nuclei grow and eventually form CDs smaller than 10 nm. During this process, functional groups such as amino and hydroxyl groups are introduced to the surface, significantly influencing their optical characteristics.[32,33] Thus, the synthesis method directly impacts the size, structure, and luminescence behavior of CDs. Advances in synthesis techniques have led to two main approaches: top-down and bottom-up.[34–36] Top-down methods fragment bulk carbon materials (*e.g.*, graphite and carbon nanotubes) into nanoscale particles through physical or chemical

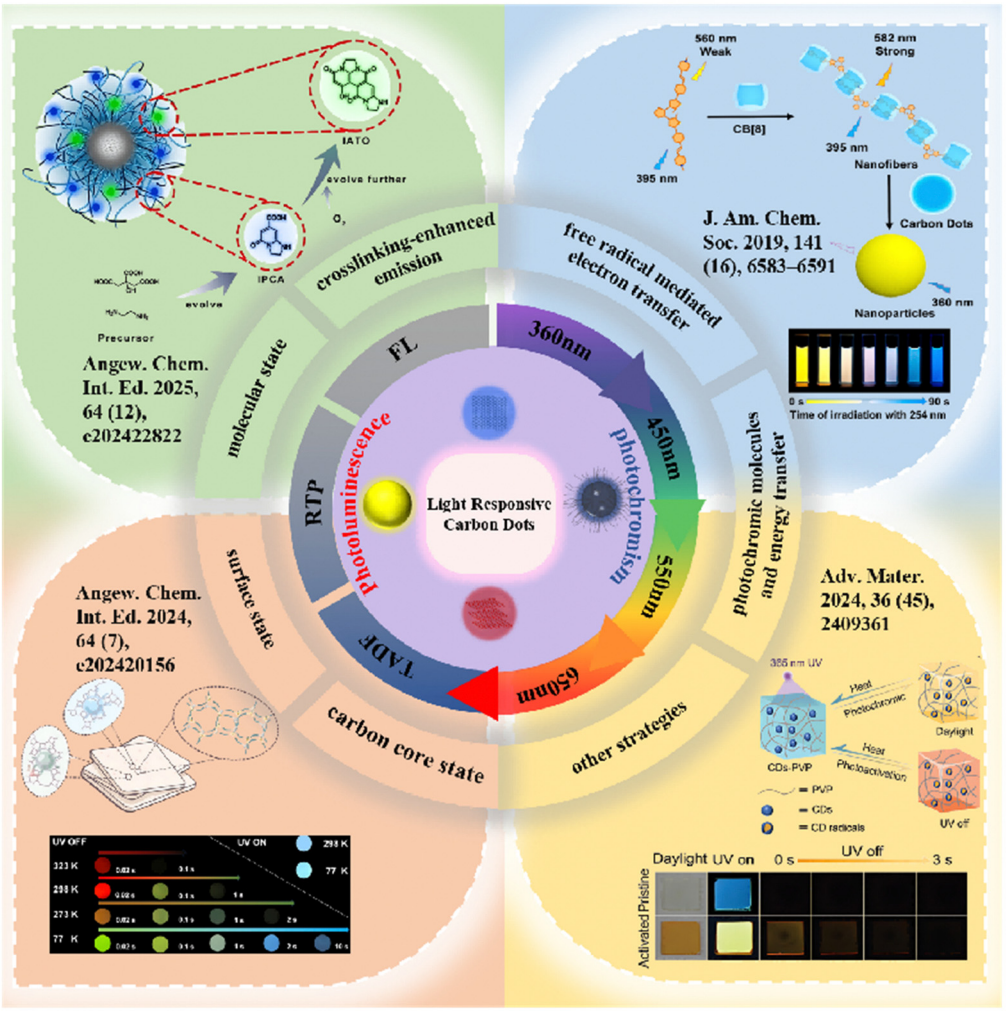

Fig. 1 Schematic timeline of key advances in light-responsive CDs. Reproduced with permission from ref. 24–26 and 30. Copyright 2019, *J. Am. Chem. Soc.* Copyright 2024, *Angew. Chem., Int. Ed.* Copyright 2024, *Adv. Mater.* Copyright 2024, *Chem. Eng. J.*

processes, often resulting in CDs with a sp^2 carbon core. In contrast, bottom-up methods use small organic molecules, polymers, or biomass as precursors, employing techniques such as hydrothermal, solvothermal, or microwave-assisted synthesis to create CDs with customizable surface functionalities and varied carbon core structures.

This review focuses on the luminescence properties of photoresponsive CDs, categorizing them into photoluminescent and photochromic systems. Photoluminescent CDs include those exhibiting fluorescence, RTP, and TADF. By integrating insights into the structure of CDs with electronic transition mechanisms, this review consolidates various luminescence pathways—such as carbon core emission, molecular state emission, surface state emission, and CEE—while exploring triggering factors for photochromism, including free radicals and energy transfer. By elucidating the intrinsic relationship between the structural configurations and luminescence properties of CDs, this review provides a theoretical foundation for designing functionalized CDs tailored for specific applications in biomedicine,[37,38] optoelectronic devices,[39,40] catalysis,[41] and anticounterfeiting technologies.[42] Furthermore, it systematically summarizes the technical bottlenecks and key challenges encountered during synthesis processes and practical applications of photoresponsive CDs. Building on current technological trends, this review proposes forward-looking perspectives to foster interdisciplinary collaboration and in-depth research, ultimately aiming to accelerate the translation of CDs-based innovations from fundamental investigations to industrial-scale applications.

2. Classification of light-responsive carbon dots by luminescence properties

2.1 Photoluminescent carbon dots

Photoluminescent CDs refer to CDs that, after absorbing light of a specific wavelength (such as ultraviolet light), emit light of different wavelengths in the form of fluorescence or RTP. This luminescence behavior originates from complex electronic transition processes within the CDs, and its mechanism is closely related to their structure, composition, and preparation methods. Currently, most scholars attribute the luminescence mechanisms of CDs to four main types: the carbon core state, surface state, molecular state, and CEE (vibration restriction through cross-linking to improve luminescence efficiency, mainly used in CPDs).[43–45] On the basis of differences in luminescence lifetime and excited-state transition mechanisms, photoluminescent CDs can be divided into three categories: (a) short-lifetime fluorescence, (b) long-lifetime RTP, and (c) TADF. Fluorescent CDs absorb light across specific wavelengths. When photons of a specific wavelength are absorbed, they excite electrons from the ground state to an excited state. The electrons return to the ground state *via* radiative transitions, emitting fluorescence.[46,47] Phosphorescent CDs absorb photons and subsequently enter the triplet excited state (T_1) *via* intersystem crossing (ISC). Their characteristic long-lived emission (microseconds to seconds) results from the slow $T_1 \rightarrow S_0$ transition. For example, at room temperature, when CDs are excited by ultraviolet light, they continue to exhibit orange RTP for a period after the excitation source is turned off. Typically, this process requires stabilization—often achieved through a hydrogen-bond network or a rigid matrix—to suppress nonradiative transitions and enhance the RTP effect.[12,48,49] TADF CDs undergo a slightly different process. After electrons are excited to the excited state, they undergo ISC from the singlet excited state to the T_1. Because the energy difference between the singlet and triplet states is extremely small, thermal activation (for example, at ambient temperature) allows the triplet excited electrons to acquire enough energy to undergo reverse intersystem crossing (RISC) from T_1 back to S_1. Finally, the electrons return to the ground state, emitting delayed fluorescence.[14,15]

2.2 Photochromic carbon dots

Photochromic CDs reversibly modulate their optical properties *via* structural or electronic state changes under specific wavelength illumination. Their core mechanism is based on the synergistic effect of photoinduced electronic transitions and dynamic molecular structural changes, which is manifested in significant alterations in both absorption and emission spectra.[50,51] The key feature of these materials is that photoexcitation triggers a reversible molecular-level reconstruction, thereby enabling precise control over the color and intensity of fluorescence and RTP. The photochromic behavior of CDs involves several mechanisms, including energy transfer modulation, free radical-mediated electron transfer, and photoinduced redox processes.[29,52,53] Among these, energy transfer modulation is a key mechanism that involves the interaction of photosensitive molecules with CDs. In energy transfer modulation, photosensitive molecules—such as SP and diphenylethene—interact with CDs *via* Förster resonance energy transfer (FRET) to achieve luminescence modulation. For example, SP undergoes ring-opening isomerization to form MC under ultraviolet irradiation.[54] The free radical mechanism, on the other hand, involves the generation of unpaired electrons on the surface of CDs or within embedded molecules induced by light, which alters the electronic structure of the material. For example, CDs modified with NIs form radical anions under illumination, leading to a redshift in the absorption band.[31] Environmental factors such as oxygen and humidity regulate the formation and quenching of these radicals; oxygen quenches triplet excitons, thereby inhibiting afterglow, whereas an inert atmosphere can significantly enhance the luminescence performance. Other designs, such as composite CDs, take advantage of the physical constraints and chemical bonds provided by the matrix material (*e.g.*, SiO_2 or polymer) to stabilize the photosensitive molecules on the CDs and enhance their photoresponsive properties.[27,55,56] In summary, the mechanisms underlying the photochromic behavior of CDs are diverse, encompassing molecular structural rearrangements, changes in electronic states, and interfacial effects, thereby offering abundant possibilities for applications in dynamic information encryption, light-controlled devices, and beyond.

3. Synthesis methods for photoresponsive carbon dots

Since the discovery of CDs, which have undergone nearly two decades of development, two synthetic routes, top-down and bottom-up, have been developed, and their synthetic choices directly affect the carbon core structure, surface functional groups, and functionality of CDs. Top-down methods fragment bulk carbon sources (*e.g.*, graphite, and carbon nanotubes) into nanoscale CDs, forming sp^2-hybridized graphite microcrystalline cores. Common techniques include laser ablation, chemical oxidation, and ultrasonication.[34,57–62] On the other hand, bottom-up methods typically use small molecules or polymers as precursors and employ techniques such as hydrothermal, solvothermal, pyrolysis, and microwave-assisted methods to construct sp^2/sp^3 hybridized amorphous or polymeric network carbon cores, offering advantages such as diverse surface functional groups ($-NH_2$, –OH, *etc.*) and flexible *in situ* functionalization.[63]

3.1 Top-down method

3.1.1 Arc discharge method. The discovery of CDs can be traced back to the preparation of carbon nanotubes (SWNTs) *via* arc discharge. Xu *et al.* discovered two nanomaterials during gel electrophoresis purification of single-walled carbon nanotubes: short carbon tubes and fluorescent nanoparticles.[3] This discovery marked the early recognition of CQDs. After further dialysis and purification, these fluorescent nanoparticles were divided into three different size components, which exhibited blue-green, yellow, and orange fluorescence under 365 nm UV light excitation. This discovery not only provides a new method for separating nanomaterials but also lays the foundation for the study of the properties of CQDs. However, there are significant limitations in using electrophoresis to prepare CQDs: although this method allows for the screening of different sizes of CDs, the purity of the products is often low, and the isolated particles are usually larger than 10 nm, making it difficult to effectively demonstrate quantum confinement effects.[64,65]

3.1.2 Laser ablation method. Laser ablation bombards carbon sources (*e.g.*, graphite and carbon targets) with high-energy lasers, inducing decomposition or exfoliation under localized high-temperature and high-pressure conditions to generate CDs. The core processes include material decomposition, nanoparticle formation, and surface modification. In 2006, Sun *et al.* synthesized quantum-sized CDs *via* laser ablation and surface modification.[66] They first used laser ablation technology in an argon atmosphere containing water vapor to prepare carbon nanoparticles and then surface-modified the carbon particles after acid treatment and successfully achieved photoluminescence *via* organic small molecules (such as PEG1500N). These CDs had a diameter of approximately 5 nm and exhibited strong photoluminescence characteristics, with emission wavelengths spanning from the visible to near-infrared (NIR) regions and QYs reaching over 4%. Hu *et al.* developed a one-step method to synthesize fluorescent CQDs by laser irradiation of carbon powder in organic solvents.[62] By selecting appropriate solvents, they could simultaneously achieve the formation and surface modification of CQDs, as well as tuning their photoluminescence properties. This method has demonstrated great potential for the preparation of novel luminescent materials. Cui *et al.* used dual-beam pulsed laser ablation on low-cost carbon cloth targets to produce homogeneous CQDs with a QY of up to 35.4%.[35] These CDs exhibited stable photoluminescence properties, with an emission peak at 448 nm, and their photoluminescence emission was independent of the excitation wavelength. Thus, laser ablation is an efficient and clean method for preparing CDs and is particularly suitable for the rapid synthesis of high-purity, tunable CDs. However, its synthesis process is more complex, with low carbon source utilization, and the size distribution of the CDs produced is not uniform, requiring further separation.

3.1.3 Oxidation method. The oxidation methods for synthesizing CDs mainly include chemical oxidation and electrochemical oxidation methods. The chemical oxidation method involves etching or oxidative polymerization of carbon sources by strong oxidizing agents to form nanoparticles with fluorescent properties. Tian *et al.* obtained nanoscale carbon particles by refluxing soot from natural gas in concentrated nitric acid for 12 hours.[58] After neutralization and dialysis, the particles exhibited good water solubility and photoluminescence properties, with a QY of 0.43% and an emission peak at 420 nm, with fluorescence originating from surface state electronic transitions. Moreover, these nanoscale carbon particles also displayed electrochemical activity. Another representative study by Peng *et al.* treated carbohydrates (such as glucose, sucrose, or starch) with concentrated sulfuric acid for dehydration and then used nitric acid to decompose them into CDs, followed by amination with compounds (such as TTDDA) for surface passivation, thereby obtaining multicolor fluorescent CDs.[67] Dong *et al.* proposed a method to extract oxidized CDs from activated carbon by oxidizing activated carbon with concentrated nitric acid and then dialyzing to remove impurities, ultimately achieving a yield of over 10%.[68] Yan *et al.* developed a convenient chemical oxidation method using starch as a precursor and treated it with high-temperature carbonization and oxidants, yielding water-soluble CQDs with bright blue fluorescence and a QY of 11.4%.[57]

In the electrochemical synthesis of CDs, a carbon source (such as graphite or organic material) is used as the anode, and a voltage is applied in the electrolyte, causing oxidation at the anode to generate nanoscale CDs. In 2007, Zhou *et al.* synthesized blue-emitting carbon nanocrystals *via* the electrochemical treatment of multiwalled carbon nanotubes (MWCNTs), achieving a QY of 0.064 with an emission peak at 410 nm.[69] Li *et al.* also used electrochemical methods to treat MWCNTs, obtaining uniform carbon nanocrystals with a QY of 0.064 and an emission peak at 410 nm, indicating good water solubility and photostability.[60]

3.2 Bottom-up method

3.2.1 Solvothermal method. The solvothermal process facilitates precursor carbonization, condensation, and surface functionalization under high-temperature, high-pressure conditions in a sealed reactor, ultimately forming fluorescent carbon nanoparticles. The choice of solvent plays a critical role

in tuning the properties of the product (such as fluorescence, surface functional groups, and particle size distribution). The solvent composition can be divided into single-solvent and mixed-solvent categories, which differ significantly in their mechanisms and applications. Single solvents (such as ethylene glycol, acetone, or *N*,*N*-dimethylformamide (DMF)) have high boiling points and strong solvency, allowing them to maintain a liquid state under high temperature and pressure, thus promoting the carbonization and condensation of the precursors.[63,70,71] For example, Ding and colleagues dissolved L-glutamic acid and *o*-phenylenediamine (*o*-PDA) in various solvents (including formamide, DMF, ethanol, and aqueous sulfuric acid) to achieve CDs with continuously tunable emission wavelengths—from blue (443 nm) to NIR (745 nm).[72] Here, the choice of solvent not only affected the particle size but also affected the ratio of oxygen- and nitrogen-containing surface groups, which in turn influenced the number of surface defects. By carefully selecting the solvent, it was possible to minimize these defects and enhance the optical properties of the CDs (Fig. 2a). Qin *et al.* used anhydrous ethanol as the solvent to adjust the temperature and time of the solvothermal reaction, synthesizing multicolor fluorescent CDs from a single biomass precursor (moss). The emission wavelengths shifted from red to blue, with red emission decreasing and blue emission increasing as the reaction conditions varied. In another study, Liu and coworkers used perylene tetracarboxylic dianhydride (PTCDA) and urea in DMF to synthesize CDs featuring an extensive conjugated carbon core.[73] The inclusion of DMF promoted the fusion reaction between PTCDA and urea, enabling the CDs in aqueous solution to exhibit a main absorption peak at 720 nm and an emission peak at 745 nm in the NIR region (Fig. 2b). Sun *et al.* synthesized CDs using CA and Nile blue A as thermally generated precursor solvents. Precise control of the degree of carbonation was achieved by adjusting the type of solvent (water or ethanol) used.[74] In particular, ethanol, as a low-boiling solvent, was able to promote a vigorous carbonation process, resulting in the formation of red CDs with large conjugated domains. In contrast, water, as a high-boiling solvent, was able to inhibit the carbonation process and generate blue CDs with small sizes. The blue CDs exhibit excitation dependence due to the presence of more defects on the surface, whereas the red CDs exhibit excitation processes independent of the excitation wavelength due to their uniform conjugated domains (Fig. 2c).

Multiple mixed solvents are integrated to optimize the reaction rate and product uniformity. For example, Tian *et al.* used a mixed solvent of water, glycerol, and DMF to successfully synthesize full-color-emitting CDs,[75] and by adjusting the solvent ratio, the CDs exhibited full-color emission ranging from 448 to 638 nm in solution, with a PLQY between 30% and 40% (Fig. 2d). Lu *et al.* used a binary system of water and formamide

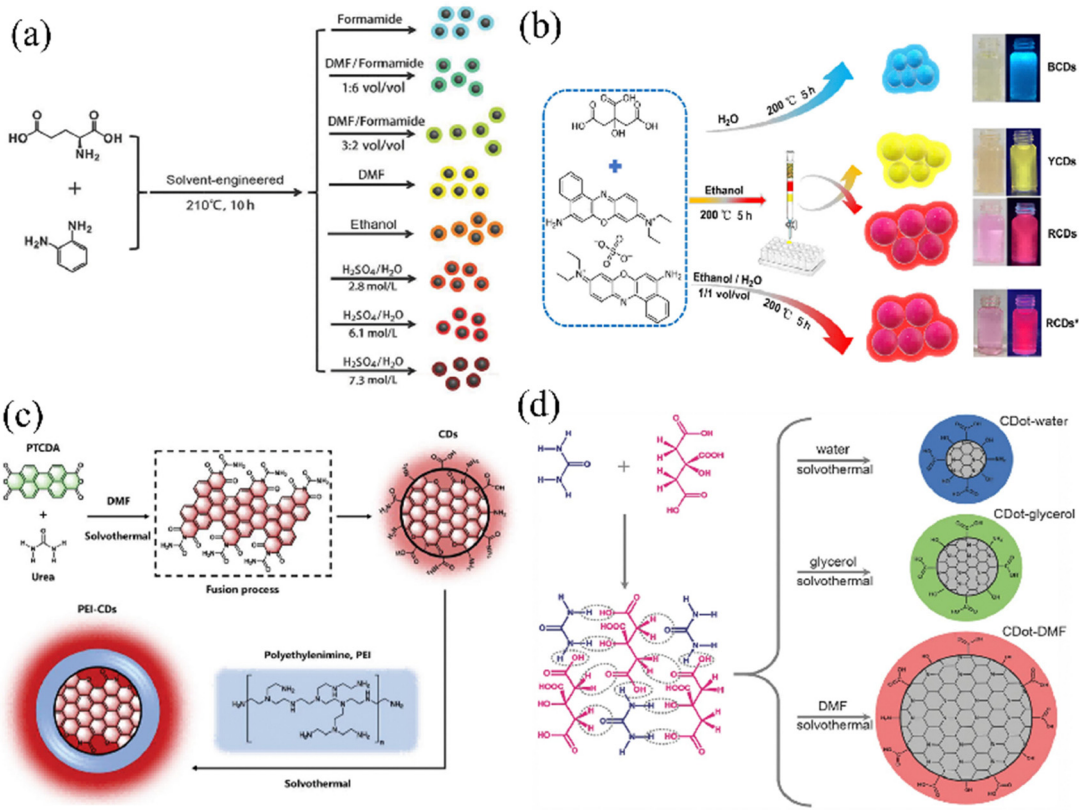

Fig. 2 (a) Single-solvent emission tuning *via* defect and size control. Reproduced with permission.[72] Copyright 2018, Wiley-VCH. (b) DMF-driven NIR CDs with conjugated carbon cores. Reproduced with permission.[73] Copyright 2022, Wiley-VCH. (c) Water (blue, excitation-dependent) *vs.* ethanol (red, excitation-independent) CDs. Reproduced with permission.[74] Reproduced with permission. Copyright 2021, Springer Nature. (d) Mixed-solvent full-color and dual-color CDs for ion detection. Reproduced with permission.[75] Copyright 2017, Wiley-VCH.

with CA and ethylenediamine as precursors to synthesize dual-color (blue and red) CDs.[76] These CDs were incorporated into ion-imprinted fluorescent polymers for dual-channel detection of Cr^{3+} and Pb^{2+}:Cr^{3+} selectively quenches blue fluorescence, whereas Pb^{2+} quenches red fluorescence, and Pb^{2+} quenches only red carbon dot fluorescence.

3.2.2 Hydrothermal method. Hydrothermal synthesis offers an eco-friendly and efficient strategy for preparing CDs. High-temperature and high-pressure conditions drive precursor dehydration, polycondensation, and carbonization, yielding fluorescent CDs with uniform size and functionalized surfaces.[77–79] This method offers advantages such as mild reaction conditions, a wide range of raw materials, and no need for complex postprocessing, making it particularly suitable for large-scale preparation and doping control. In terms of precursor selection, biomass resources (*e.g.*, yam and loofah) contain abundant carbon, nitrogen, and sulfur, enabling direct synthesis of heteroatom-doped CDs. For example, Li *et al.* used yam as a carbon-nitrogen source and synthesized blue NCDs with a QY of up to 9.3% through a one-step hydrothermal method. Organic small molecules (such as CA/ethylenediamine and polyethyleneimine (PEI)) can be used to construct CPDs *via* carbonization.[80] The Zhu team developed a CA–ethylenediamine system with a carbon dot QY as high as 80%.[81] Additionally, inorganic salt combinations (such as sodium thiosulfate/sodium citrate) enable the regulation of sulfur doping. Cui *et al.* synthesized fluorescent CDs with different optical properties, including blue (B-CDs), yellow (Y-CDs) and red (R-CDs), by reacting benzene diamine isomers (*o*-PDA, *m*-PDA, and *p*-PDA) as precursors *via* a hydrothermal method at different concentrations, temperatures and time conditions.[82] The precursor concentration critically influenced CDs fluorescence intensity, peaking at 2 mg mL^{-1} but declining at higher concentrations due to self-quenching. In addition, the reaction temperature has an important effect on the optical properties of the CDs. A high temperature contributes to the carbonization and graphitization of the precursors, which affects the electronic structure and optical properties of the CDs. Lower temperatures favor amorphous carbon formation, whereas higher temperatures enhance graphitization, thereby modulating fluorescence wavelengths and QY (Fig. 3a). By hydrothermal heating at 200 °C for 2 h, Wei *et al.* successfully synthesized panchromatic photoluminescent CDs with dual concentration and excitation dependence using CA and formamide as carbon sources.[83] This kind of CDs showed a change in the fluorescence emission wavelength from 450 to 650 nm when the excitation wavelength was increased from 370 to 600 nm, covering almost the whole visible spectrum. This excitation dependence allows the CDs to emit light of different colors under different excitation conditions, thus achieving true panchromatic luminescence (Fig. 3b). In RTP, multicolor luminescence can be achieved by controlling the reaction temperature

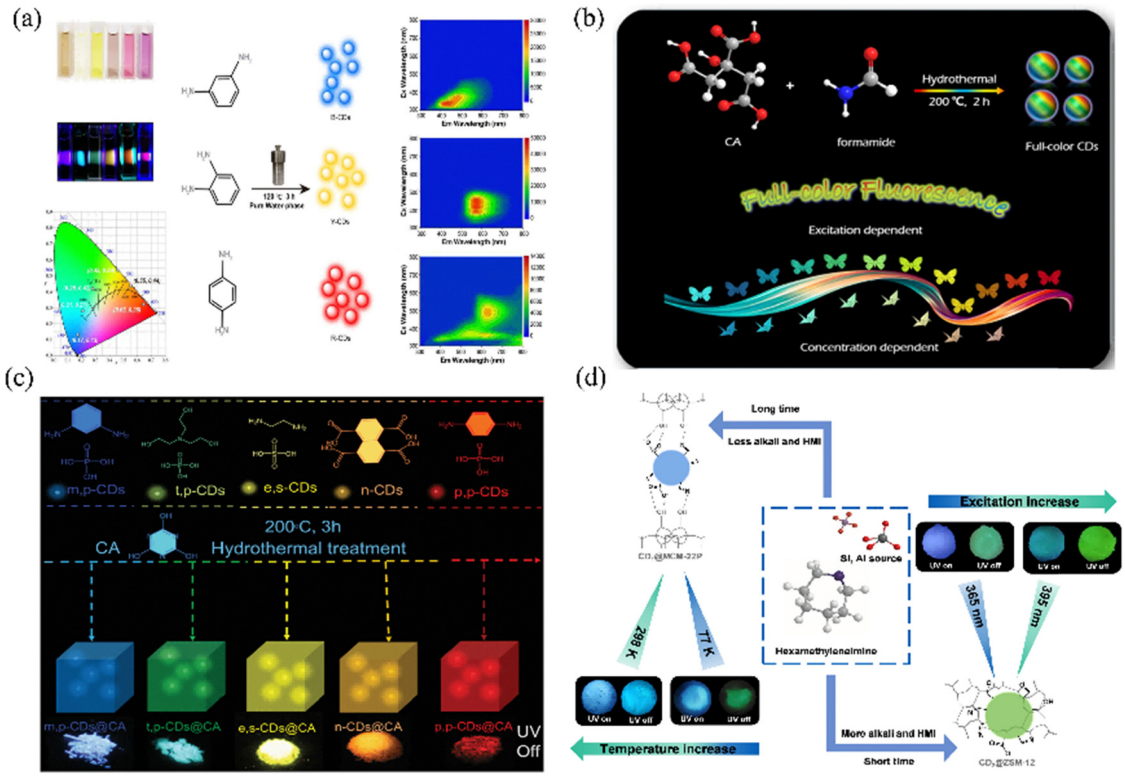

Fig. 3 Strategies for modulating multicolor luminescence in CDs *via* hydrothermal synthesis. (a) Effect of precursor concentration and temperature on the fluorescence properties of CDs. Reproduced with permission.[82] Copyright 2019, American Chemical Society. (b) Dual concentration- and excitation-dependent panchromatic photoluminescence of CDs. Reproduced with permission.[83] Copyright 2022, Elsevier. (c) Multicolor RTP achieved by embedding CDs in a rigid cyanuric acid matrix. Reproduced with permission.[13] Copyright 2022, Wiley-VCH GmbH. (d) Temperature- and excitation-dependent afterglow in CD–zeolite composites. Reproduced with permission.[84] Copyright 2023, Tsinghua University Press.

and time. In this process, the hydrothermal method promotes the crystallization of RTP. This network can effectively isolate oxygen and suppress nonradiative decay. Moreover, it regulates the surface functional groups of CDs (such as C═O/C═N), enhances spin–orbit coupling (SOC), and improves RTP efficiency (Fig. 3c). Wen *et al.*[84] synthesized two CD–zeolite composites (CD_1@MCM-22P and CD_2@ZSM-12) *via* a one-step hydrothermal method, in which CD_1@MCM-22P was reacted for 4 days at 160 °C, while CD_2@ZSM-12 was reacted for 3 days at 160 °C during the preparation process, and temperature-dependent and excitation-dependent multicolor afterglows were realized. CD_1@MCM-22P exhibited blue TADF at low temperatures (77 K) and shifted to green RTP when the temperature was raised to 298 K. CD_2@ZSM-12 exhibited blue fluorescence under 254 nm excitation and shifted to green RTP under 365 nm excitation. Hydrothermal treatment modulates the degree of carbonization and surface functional groups, optimizing the material optical properties. Moreover, the rigid domain-limiting effect of the zeolite matrix helps to stabilize the triplet excitons, which in turn prolongs the RTP lifetime (Fig. 3d).

3.2.3 Microwave-assisted method. Microwave-assisted synthesis enables rapid and efficient CDs preparation. This method heats the polar molecules in the reaction system directly through microwave irradiation, causing the precursor materials to undergo carbonization and functionalization in a very short time.[85,86] For example, Hao *et al.* employed a microwave-assisted method in which CA, urea, and NaOH were used as precursors.[87] After three minutes of heating, they successfully prepared CDs in four luminescent modes (fluorescence, upconversion photoluminescence, RTP, and chemiluminescence). In the solid state, these CDs exhibited bright fluorescence, upconversion photoluminescence, and RTP, as well as high-efficiency chemiluminescence properties in a chemiluminescent system. In recent years, microwave-assisted methods have demonstrated the advantages of rapid reactions, precise structural modulation and large-scale production in the controlled synthesis of CDs. For example, Wan *et al.*[88] used trimellitic anhydride and piperazine as precursors to synthesize yellow fluorescent CDs *via* the microwave method, resulting in a solution QY of 6.14%, which was much lower than that of 58.35% in the solid-state because of the suppression of molecular vibration in the solid-state environment (Fig. 4a). Ding and colleagues adjusted the PMDA-to-*o*-PDA ratio and applied microwave-assisted heating for 10–20 minutes, resulting in CDs with solid-state full-color emission ranging from 438–633 nm.[89] Notably, this method achieved kilogram-scale production at a rate of 0.97 kg per hour. By altering the amount of PDA and

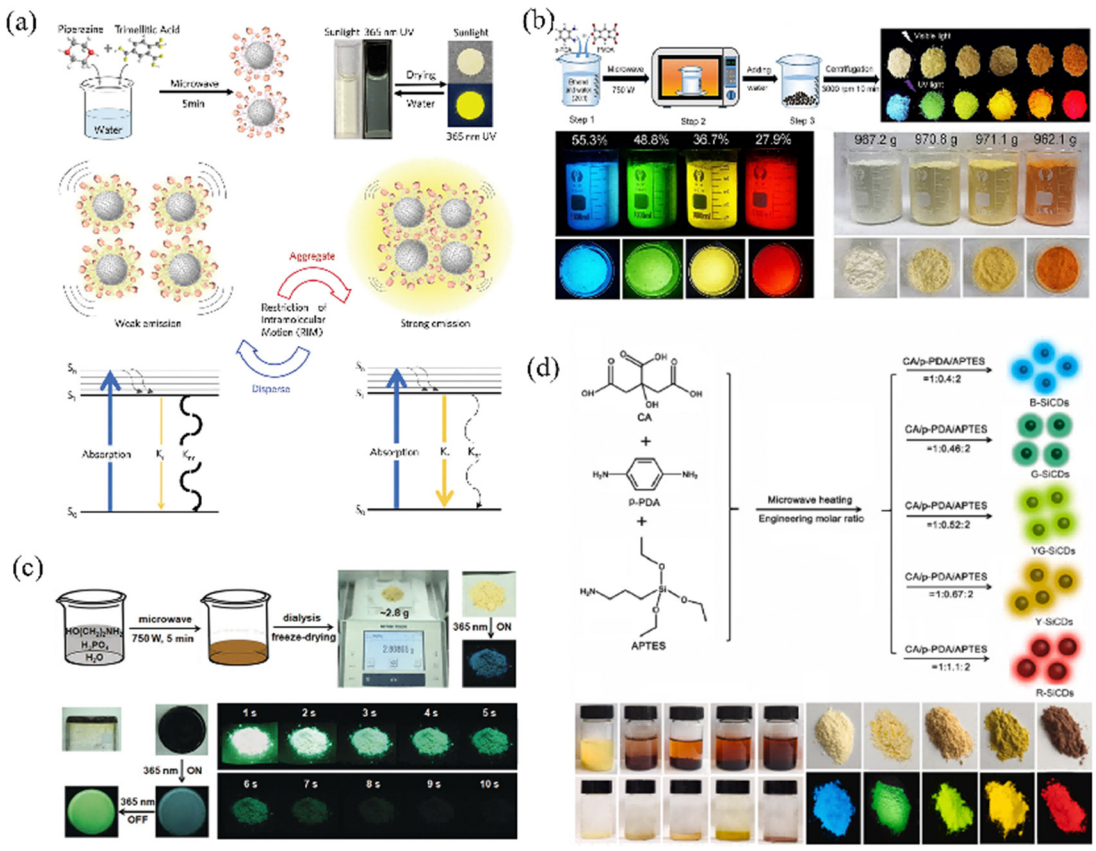

Fig. 4 (a) Yellow fluorescent CDs synthesized *via* a microwave-assisted method with an enhanced solid-state QY due to suppressed molecular vibrations. Reproduced with permission.[88] Copyright 2023, Wiley-VCH. (b) Full-color solid-state emissive CDs achieved through PMDA/*o*-PDA ratio modulation and kilogram-scale production. Reproduced with permission.[89] Copyright 2022, Elsevier. (c) N, P-codoped CDs exhibiting blue emission and long-lived solid-state RTP *via* phosphorus-enhanced ISC. Reproduced with permission.[85] Copyright 2018, Wiley-VCH. (d) Silane-functionalized SiCDs with tunable emission *via* particle size and graphitic nitrogen control. Reproduced with permission.[90] Copyright 2022, Elsevier.

reaction time, the solid-state emission wavelength can range from 438–633 nm, which is challenging for traditional synthesis (Fig. 4b). Jiang's team developed N- and P-codoped CDs from ethanolamine and phosphoric acid,[85] and the solution-state blue emission (QY = 20.52%) originated from the n → π* transition. The solid-state RTP lifetime reached 1.46 s, but the QY decreased to 3.53%, confirming that phosphorus doping promoted the enhancement of the intersystem tunneling efficiency and aggregation-induced quenching effect (Fig. 4c). Hu *et al.*[90] rapidly generated SL-functionalized SiCDs by heating for ten minutes *via* a microwave-assisted method in which CA, *p*-PDA, and APTES were used as precursors. By adjusting the amount of *p*-PDA, it was possible to control the particle size and nitrogen doping of the CDs, which in turn enabled the emission wavelength of the CDs to be adjusted from 438 to 633 nm. This redshift was attributed to increased particle size and graphitic nitrogen content (Fig. 4d).

3.2.4 Pyrolysis method. Pyrolysis decomposes organic precursors under high-temperature, oxygen-free or inert gas conditions to carbonize materials.[91] Elements such as C, H, and O in organic molecules undergo dehydration and condensation reactions to form the carbon core, ultimately generating nanoscale CDs.[92] In 2006, the Bourlinos team pioneered the pyrolysis method for carbon dot synthesis: by using CA as the carbon source and organic amines as surface modifiers, they achieved covalent bonding between the organic shell and the carbon core *via* amide bond (–NHCO–) formation during pyrolysis.[93] The CDs prepared by this method had a particle size of approximately 7 nm and exhibited a nearly spherical morphology.

The pyrolysis method offers significant process simplification advantages. For example, Hu *et al.*[94] used a simple pyrolysis strategy to construct Si–CDs@B_2O_3 nanocomposites. The Si–CDs@B_2O_3 exhibited persistent RTP for hours, and the RTP mechanism was attributed to the covalent bonding between B_2O_3, SiO_2, and the CDs. Li *et al.*[95] used *meta*-hydroxybenzaldehyde as a precursor and synthesized multicolored-emitting CDs *via* the pyrolysis method under different reaction conditions. The precursor formed different reaction pathways under acidic or basic conditions, producing molecules with varying conjugated structures, which enhanced the photoluminescence upon formation of the CDs. Miao *et al.*[96] controlled the pyrolysis temperature and ratio of CA and urea to synthesize CDs that emitted blue, green, and red light. The emission wavelength could be adjusted in the range of 430–630 nm, depending on the degree of graphitization and changes in the number of surface carboxyl groups.

Pyrolysis also offers green synthesis, high efficiency, controllability, and versatility for CDs preparation. Gao *et al.*[97] chiral CDs were synthesized by solvent-free pyrolysis using a chiral precursor (*R*/*S*-1,1′-binaphthyl-2,2′-diamine) with urea, where the carbonyl group and the nitrogen atoms are on the surface. Reducing the singlet-triplet energy gap *via* enhanced SOC and charge transfer (CT) promotes ISC, enabling long-lived RTP (and intrinsic circularly polarized fluorescence/RTP) (Fig. 5a).

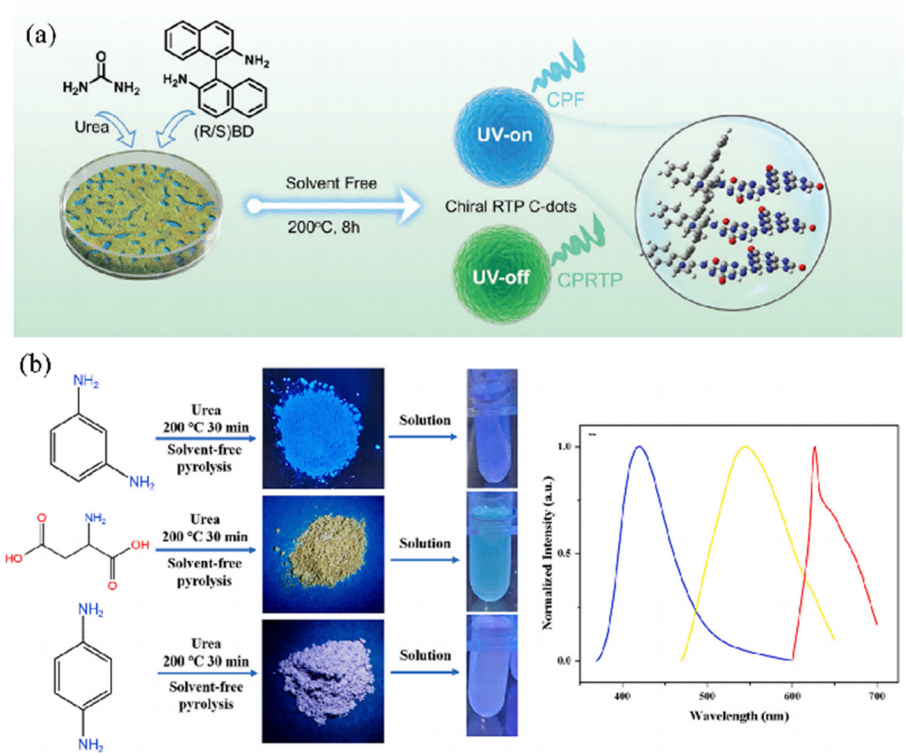

Fig. 5 (a) Chiral CDs with circularly polarized RTP *via* enhanced SOC. Reproduced with permission.[97] Copyright 2024, Wiley-VCH. (b) Solid-state multicolor CDs (blue, yellow, red) for latent fingerprint imaging, achieving 682 ms phosphorescence lifetime *via* C=N bond modulation. Reproduced with permission.[98] Copyright 2024, Elsevier.

Luo *et al.*[98] also used solvent-free pyrolysis with urea as the dispersing agent, modulated the carbon nuclei through the conjugated structures of different precursors (*m*-PDA, DL-aspartic acid, *p*-PDA), and synthesized blue, yellow and red solid-state fluorescence (Fig. 5b). Red CDs exhibit blue RTP (682 ms lifetime) due to increased C=N bonds and reduced defects. Urea suppresses π–π stacking, mitigating aggregation-caused quenching (ACQ), achieving high solid-state fluorescence intensity and applying it to latent fingerprint imaging.

3.2.5 Other methods. In addition to conventional synthesis methods, CDs can also be synthesized *via* strategies such as combustion, templating, and room-temperature synthesis methods, each with unique characteristics.

Room-temperature methods synthesize CDs *via* molecular self-assembly or solvent-induced crystallization. For example, Sun *et al.*[99] proposed a room-temperature strategy involving separate polymerization and carbonization steps to synthesize red-emissive CDs. The *o*-PDA was first polymerized in ethanol for 3 days to form amorphous PDs, followed by controlled carbonization *via* concentrated sulfuric acid, and the decoupled reaction kinetics method was used. Acetic acid additives during polymerization promoted amide group formation, enhancing CEE *via* hydrogen bonding, which optimized both the conjugation domains and surface defects. Similarly, Wang *et al.*[100] demonstrated the chemical synthesis of multicolor CDs entirely at room temperature: blue (B-CDs) from glucose/NaOH, green (G-CDs) *via* increased C–O bonds *via* the addition of *p*-phthalaldehyde, and red (R-CDs) through amino–N energy levels introduced by *m*-diethylaminophenol. The hydroxyl-rich surface of the G-CDs extended the fluorescence lifetime to 20.65 ns, whereas nonradiative recombination in the R-CDs limited the efficiency, highlighting the role of surface group engineering in optical tuning. In contrast, room-temperature synthesis methods were used to prepare CDs at ambient temperature through molecular self-assembly or solvent-induced crystallization. Yan *et al.*[101] achieved rapid (3 h) synthesis of yellow-green CDs *via* Schiff base formation between glyoxal and OPD under strongly alkaline conditions (Fig. 6a). The abundant amino/hydroxyl groups enabled tetracycline detection *via* the inner filter effect (IFE), with a linear range of 10–400 μM (LOD 6.0 μM), revealing how surface functionalization directly impacts both emission and sensing applications. Compared with high-energy methods, these room-temperature strategies are energy-efficient and align with green chemistry principles.

In contrast, combustion methods can rapidly generate CDs through the combustion of organic materials, although they require precise control over the reaction conditions. Zhang *et al.*[105] successfully synthesized CDs *via* combustion methods with flammable organic materials such as ethanol, butanol, household candles, and benzene as precursors. The size, surface groups, and fluorescence properties of the CDs were significantly influenced by the precursor carbon chain length and solvent polarity. CDs synthesized with short carbon chain precursors (such as ethanol) show stronger fluorescence at longer wavelengths (530 nm), whereas CDs made from longer carbon chains or aromatic precursors (such as benzene and candles) exhibit complex emission peaks at shorter wavelengths. Rong *et al.*[102] prepared boron and nitrogen codoped CDs using aminophenylboronic acid as the raw material. The high-temperature combustion process enabled rapid carbonization to form smaller CDs with enhanced quantum-limited-domain effects (Fig. 6b). However, the relatively low QY (1.6%) of these dots may be attributed to incomplete carbonization or excessive surface defects. Despite challenges in controlling oxygen levels and combustion temperatures, this method enables rapid synthesis of photostable CDs.

Template-based synthesis employs organic/inorganic matrices to direct CDs formation while controlling particle morphology and

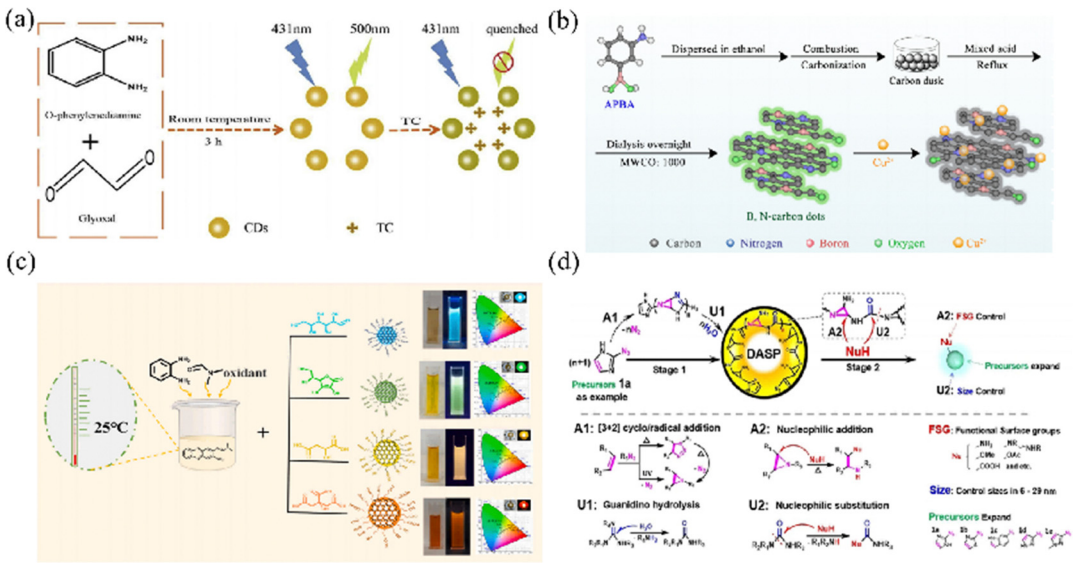

Fig. 6 (a) Yellow-green CDs for tetracycline detection *via* alkaline Schiff base formation. Reproduced with permission.[101] Copyright 2019, Elsevier. (b) B, N-doped green CDs *via* ethanol combustion and acid reflux. Reproduced with permission.[102] Copyright 2017, Elsevier. (c) Oxidant-modulated CDs with tunable bandgap and emission. Reproduced with permission.[103] Copyright 2024, Elsevier. (d) Template-guided CDs with controllable surface groups. Reproduced with permission.[104] Copyright 2020, Wiley-VCH.

size. Xu *et al.*[103] used *o*-PDA as a precursor, DMF as a solvent, and different oxidants (HNO_3, H_2O_2), polyols, or polyacids to regulate the fluorescence color of the CDs (Fig. 6c). Emission wavelengths depend primarily on particle size, graphitization degree, and conjugated systems, which collectively modulate the bandgap. Surface functionalization and elemental doping further tune the bandgap, inducing emission redshifts. Huo *et al.*[104] used a double-active-site polymer as a template and reacted it with nucleophilic reagents (such as ethylenediamine) to perform nucleophilic addition and substitution reactions, cleaving the template and forming CDs with tunable surface functional groups and sizes (Fig. 6d). These diverse synthetic strategies not only expand the controlled synthesis pathways of CDs but also provide significant theoretical and technical support for the study and application of custom optical properties of CDs by precisely regulating their structure, surface chemistry, and optical characteristics.

To understand the pros and cons of CD synthesis methods, Table 1 sums up key parameters of each method, including precursor type, reaction conditions, yield, scalability, and optical performance, enabling quick comparison.

4. Light-responsive mechanism exploration

4.1 Photoluminescence mechanism

Photoluminescence of CDs includes fluorescence, RTP and TADF.[123,124] Fluorescence arises from rapid ground-state recovery after light absorption, with emission typically occurring on a nanosecond timescale, demonstrating efficient and instantaneous light-responsive characteristics. In contrast, RTP involves an electronic jump from the triplet state to the ground state, resulting in a significantly longer emission time, lasting even seconds or more, thus providing a long-lasting optical signal. TADF is a special emission mechanism between the two, where electrons are thermally activated to return from the triplet state to the singlet state and then emit light, with emission times typically ranging from microseconds to milliseconds. To better understand and optimize the photoluminescence performance of CDs, researchers have proposed four main emission mechanisms: carbon core emission, molecular state emission, CEE, and surface state emission.[125] Importantly, these mechanisms are complementary when the emission origin and regulation of CDs are studied. The exploration of these mechanisms not only clearly reveals the luminescence origin of CDs but also provides technical support for controlling their optical properties.

4.1.1 Carbon core emission. The carbon nucleation state emission of CDs mainly originates from the conjugated structure formed by sp^2 and sp^3 hybridized carbon atoms in their core. Among them, conjugated π-systems from sp^2-hybridized carbon atoms constitute the primary luminescence mechanism. When the size of the sp^2 domains increases, the extension of the conjugated structure leads to gradual narrowing of the HOMO–LUMO energy gap, which causes a redshift phenomenon in the emission spectrum. In highly graphitized sp^2 domains, the electron jump is mainly realized by a direct $\pi \rightarrow \pi^*$ jump, which usually results in narrowband emission and a high QY. In contrast, sp^3 hybridized carbon atoms may introduce defect

Table 1 Comparison of synthesis methods for photoresponsive carbon dots

Synthesis approach	Types of carbon sources	Size and QY	Advantages	Disadvantages	Ref.
Arc discharge	Macroscopic carbon materials (*e.g.*, graphite, carbon nanotubes)	Broad size distribution, generally low QY	Scalable production	Challenging to control purity and optical properties, requires complex post-processing	3,106
Laser ablation	High-purity carbon targets (graphite, carbon cloth)	Smaller size achievable; initial QY low but improves after surface passivation	High product purity	Complex process, low carbon source utilization	107–109
Oxidation	Carbohydrates/activated carbon-based materials	Broad range of sizes and QY	Low-cost raw materials	Involves corrosive reagents, difficult size control	67,69,110
Hydrothermal	Organic small molecules/biomass	Wide size range, high QY achievable	Eco-friendly process	Long reaction time	111–113
Solvothermal	Organic small molecules/polar solvent systems	Wide size range, high QY achievable	Tunable luminescence properties	High-pressure equipment required	114–116
Microwave-assisted	Organic small molecules/biomass	Wide size range, high QY achievable	Ultrafast synthesis	Inconsistent particle size	87,117,118
Pyrolysis	Organic precursors/natural carbon sources	Broad size/QY range; emission dominated by carbon core states (high stability)	Avoids strong acids/bases	Challenging carbonization control	94,96,119
Template-assisted	Carbon-containing precursors/template materials	Uniform size but low QY	High controllability in morphology and size, high crystallinity and uniformity	Complex process and high cost, limited scalability	120,121
Combustion	Organic fuels/biomass fuels	Broad size distribution with low QY	Continuous production feasibility	Complex product composition requiring purification	102,122
Room-temperature	Organic molecules/biomass extracts	Broad size range; emission color influenced by precursor type	Low energy consumption and rapid reaction, environmentally friendly	High functionalization difficulty	99,100,103

states or localized electronic states. These defect states can act as new luminescence centers, leading to broad-spectrum or multi-peak emission.[22,66,126] By modulating the ratio of sp^2 to sp^3 hybridized structures in CDs, the energy gap of the CDs can be flexibly altered, leading to a redshift or blueshift of the luminescence wavelength. For example, Li *et al.*[127] prepared CQDs *via* an electrochemical method, with sizes ranging from 1.2 to 3.8 nm. Smaller CQDs (1.2 nm) emit ultraviolet light, medium-sized CQDs (1.5–3 nm) emit visible light, and larger CQDs (3.8 nm) emit NIR light, exhibiting a size-dependent photoluminescence (PL) phenomenon. The quantum confinement effect leads to a larger band gap as the size decreases, thus controlling the PL color. Cao *et al.*[128] successfully prepared CDs that exhibited blue and multicolor fluorescence in aqueous solution with a QY as high as 98.5% *via* ionic liquid-assisted pyrolysis of CA, catechol and oPD at low temperature and atmospheric pressure. It was confirmed by density functional theory (DFT) calculations that the quantum size effect was the key factor dominating the band gap reduction and emission redshift, which led to the expansion of fluorescence color from blue to multicolor (Fig. 7a).

Similarly, Liu *et al.*[131] used 3,4,9,10-perylene tetracarboxylic dianhydride (PTDA) as a precursor and performed hydrothermal reactions at 220 °C for 48 hours to generate CQDs. By adjusting the core size (1.5–4.5 nm), the quantum confinement effect caused the PL wavelength to shift from blue light (small size) to NIR light (large size). Huang *et al.*[132] then employed a polymer precursor strategy to synthesize size-tunable CDs by selective carbonization of star-shaped block copolymers. As the size increases, the fluorescence color shifts from blue to green, which is attributed to the redshift phenomenon due to the FRET enhancement triggered by the size increase. In this process, the quantum size effect modulates the fluorescence color by directly affecting the energy band structure. Guo *et al.*[129] synthesized full-color fluorescent CDs by optimizing hydrothermal parameters, such as temperature and catalyst, with the help of machine learning techniques (Fig. 7b). The quantum size effect indirectly regulates the size distribution of the CDs through these parameters, which in turn affects the band gap, resulting in CDs that cover the entire visible spectral range of colors, from blue to red. Yuan *et al.*[130] used CA and diaminonaphthalene as raw materials and reacted them in ethanol at 200 °C (Fig. 7c). By controlling the reaction time or adding concentrated sulfuric acid, they adjusted the carbon core size. As the core size increased, the band gap decreased, causing the emission wavelength to redshift and generate blue, green, yellow, orange, and red light in the MCBF-CQDs. Wang *et al.*[23] used *o*-PDA as a carbon source and reacted it with various acidic reagents (such as 4-aminobenzenesulfonic acid, BA) in ethanol (Fig. 7d). By modifying the surface of the CDs with electron-withdrawing/electron-donating groups and controlling the degree of carbonization and size distribution, they generated CDs with fluorescence ranging from blue to red and white, further demonstrating that the carbon core size affects the fluorescence of the CDs.

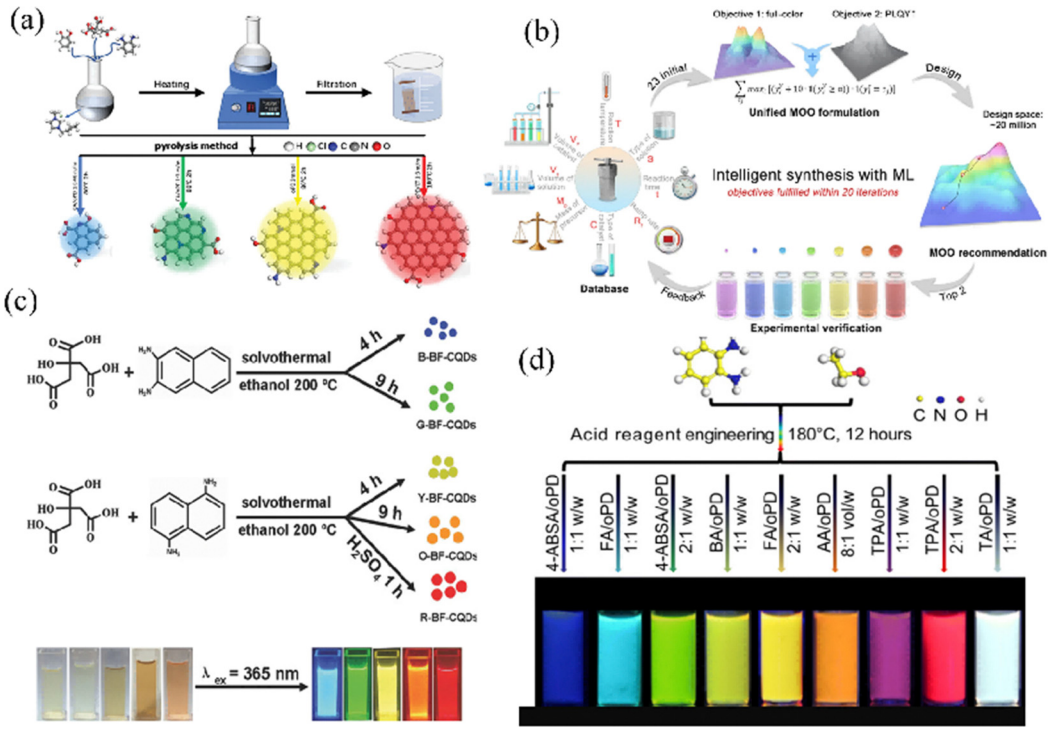

Fig. 7 (a) Ionic liquid-assisted multicolor CDs *via* quantum size effect. Reproduced with permission.[128] Copyright 2022, Wiley-VCH. (b) Machine learning-optimized full-color CDs covering the visible spectrum. Reproduced with permission.[129] Copyright 2024, Springer Nature. (c) Core-size-controlled MCBF-CQDs *via* reaction time/acid modulation. Reproduced with permission.[130] Copyright 2020, AAAS. (d) Surface-modified multicolor CDs *via* electron-withdrawing/donating groups. Reproduced with permission.[23] Copyright 2020, AAAS.

4.1.2 Molecular state emission. The molecular state luminescence mainly depends on the fluorescent groups on the surface or inside the CDs. The luminescence of many CDs is dominated by molecular fluorophores from precursors, such as IPCA, DHQP, and DAP. Liu *et al.*[95] synthesized multicolor CDs by pyrolytically modulating acid–base conditions using *m*-hydroxybenzaldehyde as a precursor. Alkaline conditions favored conjugated fluorophores (*e.g.*, DAP), whereas acid-neutral conditions yielded distinct structures (Fig. 8a). The aggregation of molecular fluorophores inhibited the movement of the fluorescence center and enhanced the luminescence of the system. In addition, the degree of conjugation of the molecular states directly determines the size of the energy gap and the emission color, whereas pH modulation of the condensation path of the precursors leads to the generation of different fluorophores. For example, a weaker green emission with sp^2 conjugation was formed under neutral conditions, whereas under alkaline conditions, the extended conjugation of DAP achieved red emission.

The electronic transition characteristics of these fluorophores directly determine the emission wavelength and efficiency. These fluorophores can be connected to the surface of the CDs, such as surface functional groups, or form fluorescent clusters, further condensing and carbonizing inside the carbon core. This fluorophore diversity was systematically revealed by Sun *et al.*,[133] who synthesized trichromatic CDs from *o*-PDA and modulated the ratio of ethanol/DMF. Using techniques such as LC–MS with NMR, BI (blue), DAP (green), and DHQP (red) were confirmed to be the molecular fluorophores (Fig. 8b). DMF inhibited the condensation pathway of DHQP through its solvent polarity, thus facilitating the generation of BI. The structure of the molecular state, such as the benzimidazole ring of BI conjugated to the phenazine of DAP, directly determines the luminescence color and QY (12% QY for BI, 23% for DAP, and 35% for DHQP). Solvent ratio adjustments altered the intermediate condensation kinetics, further demonstrating that the molecular state is the dominant factor in luminescence.

Since molecular state emission is highly sensitive to the chemical environment of the CDs' surface, researchers can achieve diverse customization of emission color and intensity by selecting different synthetic precursors or performing surface chemical modifications to introduce specific fluorophores. A striking example comes from Li *et al.*,[134] who obtained CDs by pyrolysis of poly(ethylene glycol) followed by nitrogen doping with resorcinol reflux (Fig. 8c). The C=C bonds and aldehyde groups were the fluorescence centers, and it was experimentally confirmed that $KMnO_4$ quenched the fluorescence of C=C. Nitrogen doping introduced the conjugation of the amide to the aromatic ring, and calculations revealed that the energy gap was narrowed by 0.8 eV, resulting in a redshift of the emission from 452 to 516 nm and an increase in the QY from 2.3% to 36.7%. The conjugation modification of the molecular state dominated the optical tuning rather than the carbon core size effect. The Yang research group synthesized CDs *via* CA–amine pyrolysis and isolated IPCA and its derivatives, proposing a dual emission mechanism in which molecular-state blue fluorescent groups coexist with carbon core emission. Song *et al.*[136] synthesized CDs with high QYs *via* the hydrothermal reaction of CA and ethylenediamine. This study isolated the molecular fluorophore IPCA with a blue QY of 92% and reported that the CDs are a mixture of IPCA, polymer clusters, and carbon nuclei.

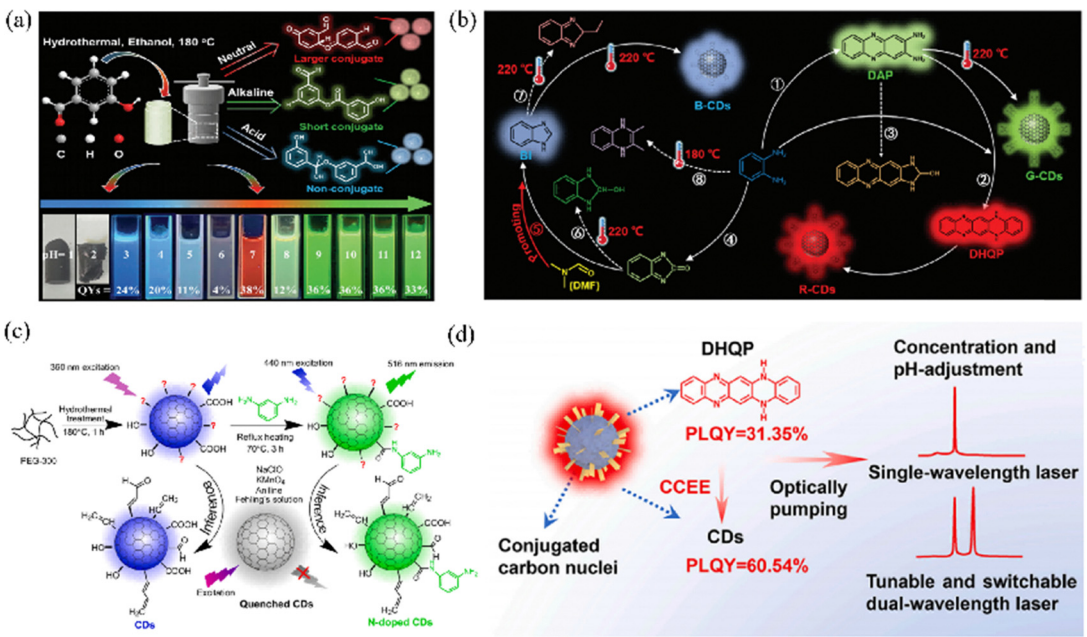

Fig. 8 (a) Acid/alkali-modulated fluorophores (DAP for red emission). Reproduced with permission.[95] Copyright 2023, Wiley-VCH. (b) Trichromatic CDs *via* solvent ratio control. Reproduced with permission.[133] Copyright 2024, Wiley-VCH. (c) Nitrogen-doped CDs with C=C/amide conjugation. Reproduced with permission.[134] Copyright 2022, Elsevier. (d) Dual-wavelength NIR CDs *via* DHQP aggregation. Reproduced with permission.[135] Copyright 2024, Elsevier.

The molecular state of IPCA dominated the high fluorescence efficiency, whereas the sp^2 domain of the carbon nuclei induced excitation wavelength dependence, with the redshift of the emission from 350 to 450 nm excitation leading to a redshift of the emission, demonstrating the coexistence and competition between the molecular and carbon core states for the luminescence pathway. Yao *et al.*[137] discovered a novel aliphatic fluorophore, 5-oxopyrrolidine-3-carboxylic acid, in CDs synthesized from CA–urea systems, which exhibited aggregation-induced emission characteristics, challenging the traditional notion that aromatic fluorophores dominate the emission. Xia *et al.* obtained AN-CPDs *via* hydrothermal polymerization carbonation of acrylamide.[138] Carbonation from 160 to 220 °C modulated the degree of cross-linking, with the nitroso functional group acting as the phosphorescent center of the molecular state. The crosslinked structure suppressed the nonradiative jump of the triplet state, the RTP lifetime increased from 61.4 ms to 466.5 ms, and the RTP wavelength redshifted from 485 to 558 nm with the extension of conjugation. The molecular states synergize with the heterostructure of the polymer to achieve tunability of the RTP.

Ren *et al.*[18] used *O*-aminophenol as a precursor to synthesize CDs through solid pyrolysis and solvothermal conversion methods. They reported that both methods produced dual-emission products. By chromatographically separating blue-emitting bCDs and yellow-emitting yCDs, they reported that both had graphene-like internal structures, with bCDs rich in amino fluorophores and yCDs rich in pyridine nitrogen fluorophores. This was the first demonstration of controlling fluorophore type (amine or pyridine nitrogen enrichment) through catalytic conditions to achieve dual-color emission from the same precursor. A similar surface fluorophore engineering strategy was employed by Zhang *et al.*[135] The NIR CDs were derived using *o*-PDA. DHQP molecules aggregated on the surface of the CDs, and the conjugated carbon nuclei increased light scattering and gain (Fig. 8d). The aggregated state of DHQP was balanced with the scattering of carbon nuclei by pH modulation, and the construction of 655 and 710 nm dual-wavelength lasers and logic gates was realized. The synergistic effect of the aggregation of molecular states and the carbon core structure enhances the stability of the gain.

These studies further reveal the crucial role of molecular state fluorophores in CDs emission and provide insight into the precise design and regulation of fluorophores to achieve different emission performances in CDs.

4.1.3 Surface state emission. The surface states critically influence the luminescence properties of CDs *via* functional groups (*e.g.*, –OH, –COOH, and $–NH_2$), defect structures, and environmental interactions. The formation of surface states primarily arises from unreacted functional groups during precursor carbonization or chemically introduced groups during post-treatment. For example, Zhu *et al.*[139] demonstrated that modulating oxygen-containing groups (C═O, C–O) through redox treatments shifts carrier recombination pathways in GQDs, leading to intrinsic (sp^2 core) emission dominating blue light emission, whereas defect state emission is suppressed. Zhou *et al.*[140] used microwave methods to prepare CDs and reported that the distribution of surface oxygen-containing functional groups (–COOH, –OH) directly affects the photocatalytic activity. For example, 2 nm CDs with high surface defect density and superoxide radical activity completely degraded organic dyes within 150 minutes. Nguyen *et al.* correlated 1–3 nm surface defects with red emission *via* STM at single-particle resolution, confirming that phenolic hydroxyl and carboxylic acid groups are the main sources of red light emission.

Strategies for regulating surface states include chemical modification, solvent effects, and defect engineering. For chemical modifications, Zhu *et al.*[141] controlled C═O (green emission) and C═N (red emission) surface states *via* redox-driven chemical modifications. Li *et al.*[142] synthesized CDs from *o*-PD and hydroquinone at room temperature, then isolated $–NO_2$/–OH-enriched Y-CDs and $–NH_2$-containing G-CDs *via* silica gel chromatography. The former achieved red light emission with a narrow bandgap and used it for detecting *p*-nitrophenol, whereas the latter could detect trace amounts of H_2O in D_2O. With respect to solvent effects, Kumari *et al.* reported that protonic solvents (*e.g.*, water) with high nitrogen doping and imine nitrogen led to red light emission, whereas in nonprotonic solvents, nitrogen doping decreased, and C–O groups were absent, leading to blueshifts. The R-CDs exhibited full visible light range emission in solvents of different polarities. In defect engineering, Zhang *et al.*[143] synthesized CDs with dual emission centers through solvothermal methods. Green/yellow emission arises from the sp^2-conjugated core, whereas red emission originates from interactions between surface oxygen groups and the core, with energy transfer between the two. Ai *et al.* modulated intramolecular hydrogen bonds *via* ligand control, adjusting the solid-state fluorescence from blue to deep red light (a span of 300 nm), which was applied in 3D-printed optical devices.

The influence of surface states on luminescence performance is reflected in the emission color, QY, and environmental responsiveness: oxygen-containing groups reduce the bandgap, causing redshifts in emission (as seen in Zhou and Zhang's studies), whereas amino groups ($–NH_2$) increase the QY *via* surface passivation (as observed in Li's study). Ding *et al.*[21] engineered cyan-functionalized CDs with AIE and RTP, achieving a 1.17 s RTP lifetime for fingerprint recognition and information encryption. Additionally, surface state optimization can enhance stability. Song *et al.*[144] embedded CDs into a $ZnAl_2O_4$ matrix and utilized energy transfer between inorganic defects and carbon dot surface states to achieve yellow-red multicolor RTP, with a lifetime of 1.05 s, allowing stable RTP under UV irradiation. In summary, surface states are central to the luminescence mechanism of CDs, and their precise regulation through chemical modification, the solvent environment, and defect engineering enables fluorescence and RTP color tuning and applications in various environments.

4.1.4 Crosslinked enhanced emission. CEE is a novel mechanism for fluorescence enhancement, where the core principle involves limiting the molecular vibrations and rotations of the emission centers through the crosslinking of polymer chains, thereby effectively reducing nonradiative energy loss and improving emission efficiency. By adjusting the crosslinking density, the

rigidity of the polymer chains, and the intermolecular interactions, the emission intensity and stability can be further optimized.[145,146]

The first report of CEE in CDs dates back to 2014, when Yang *et al.*[147] discovered the CEE effect in nonconjugated CPDs. Using branched PEI as a model system, they prepared PDs by crosslinking with carbon tetrachloride (Fig. 9a). They reported that the photoluminescence of the crosslinked PDs was significantly enhanced, which was attributed to the crosslinking restricting the vibration and rotation of the amino groups. The QY of crosslinked PDs reached 2.7%, notably higher than uncrosslinked PEI, laying the foundation for subsequent studies on CEE. In 2017, Lu *et al.*[148] broadened CEE applicability through dopamine and *o*-PD hydrothermal crosslinking, synthesizing NIR-emitting PCNDs (710 nm) and achieved two-photon fluorescence. The rigid structure formed during crosslinking polymerization effectively suppressed the motion of the chromophores and enhanced the NIR emission efficiency, providing an early example of CEE applied to long-wavelength emission. In 2022, Tao *et al.*[149] further investigated the CEE effect on CPDs. They used an "addition–condensation polymerization" strategy to synthesize CPDs with varying steric hindrances and reported that increasing steric hindrance could modulate the photoluminescence properties of the CPDs (Fig. 9b). Femtosecond transient absorption spectroscopy (TA) confirmed that the CEE effect influenced the energy level structure of the CPDs. In 2024, Xia *et al.*[150] used a combination of experimental and simulation methods to reveal the formation mechanism of CPDs. They proposed that crosslinking-induced nucleation and carbonization are the driving forces for the formation of CPDs (Fig. 9c). The experimental results revealed that the PL performance of the CPDs improved as the crosslinking agent content increased, with the highest PLQY reaching 16.25%. Zheng *et al.*[151] used 1,2,4,5-benzenetetramine (BTA) and (*E*)-2-methyl-2-butenedioic acid (MBA) as precursors to construct self-protecting CPDs *via* an amino-carboxy dehydration reaction. The amide-bonded CEE in the design enhances the SOC, facilitates ISC, and stabilizes triplet excitons to confer long-lived RTP (Fig. 9d). BTA's aromatic amine and MBA's C=C bond synergistically form a long-range conjugated domain with a narrow energy gap to lower the triplet energy level and redshift the solid-state NIR emission to 710 nm, whereas the constrained CEE framework suppresses π–π stacking to reduce nonradiative decay. These studies have deepened our understanding of the CEE effect.

4.2 Photochromic mechanism

4.2.1 Free radical-mediated electron transfer. Free radical-mediated electron transfer is a typical photochemical process. Under irradiation at specific wavelengths, functional groups on the surface of CDs or embedded molecules generate free radicals with unpaired electrons, which subsequently trigger electron transfer between molecules and significantly alter the optical properties of the material. For example, Guo *et al.*[31] synthesized CDs featuring an NI structure *via* hydrothermal treatment with 1,8-naphthalic anhydride (NA) and ethylenediamine, followed by polyvinylpyrrolidone encapsulation (Fig. 10a). Under UV irradiation, the CDs film transitioned from colorless to brown, accompanied by a shift in steady-state photoluminescence from blue to yellow and a significantly prolonged afterglow duration. This intrinsic photochromism originates from stable radicals generated through photoinduced electron transfer at electron-deficient aromatic imide groups. This study first

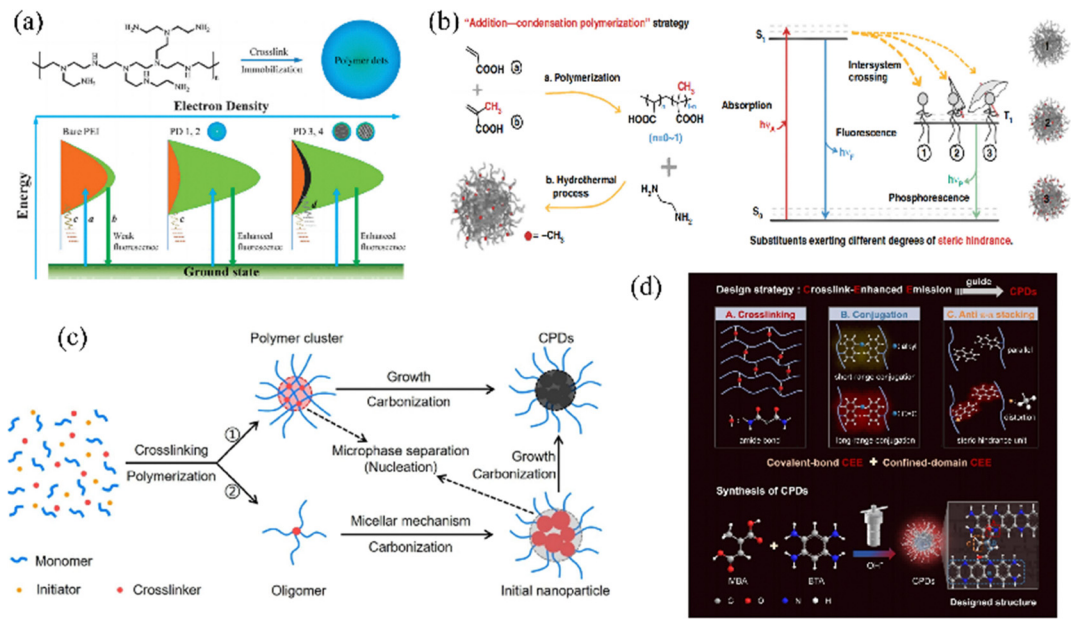

Fig. 9 (a) Non-conjugated CEE effect in PEI-based polymer dots *via* amino group restriction. Reproduced with permission.[147] Copyright 2014, RSC. (b) Confined-domain CEE modulating energy levels *via* steric hindrance. Reproduced with permission.[149] Copyright 2022, Springer Nature. (c) Crosslinking-induced nucleation-carbonization for enhanced PLQY. Reproduced with permission.[150] Copyright 2024, Wiley-VCH. (d) Self-protective NIR-RTP CPDs *via* amide-bonded CEE and triplet exciton stabilization. Reproduced with permission.[151] Copyright 2024, Wiley-VCH.

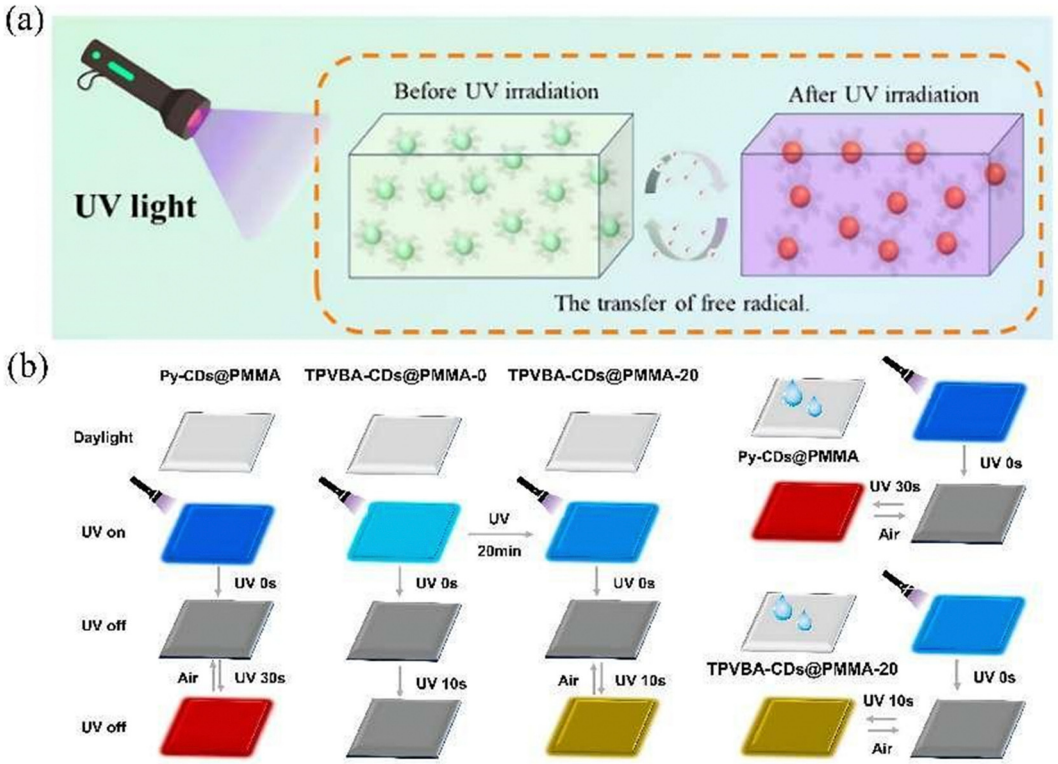

Fig. 10 (a) Continuous UV irradiation induces color change *via* free radical transfer. Reproduced with permission.[152] Copyright 2024, American Chemical Society. (b) Reversible fluorescence/RTP in TPVBA-CDs@PMMA *via* photocyclization radicals and PMMA confinement, enabling cyan blue fluorescence and yellow RTP control. Reproduced with permission.[28] Copyright 2024, Elsevier.

revealed the unique mechanism of *in situ* formation of anion radicals in NI-based CDs under photoexcitation.

Similarly, Zhang *et al.*[152] synthesized CDs from naphthalene tetracarboxylic acid, urea, and BA using a microwave-assisted method, then dispersed them in diethylenetriamine (DETN), PEI, and tetraethylenentamine (TEP) to create CDs@DETN, CDs@PEI, and CDs@TEP systems. UV irradiation shifted the fluorescence from cyan/green/bluish-green to orange-red/yellow-orange/orange-red. This change was attributed to the formation of free radical anions through a photoinduced electron transfer process, thereby achieving reversible optical regulation.

In another study, Sun *et al.*[28] synthesized two types of CDs (Py-CDs and TPVBA-CDs) *via* a microwave-assisted solid-phase reaction and made Py-CDs@PMMA and TPVBA-CDs@PMMA films by combining them with PMMA. Under prolonged UV irradiation, the tetraphenylethylene on TPVBA-CDs' surface photocyclized, generating free radicals and shifting the fluorescence color from cyan to blue. This process involved fluorescence emission peak shifts, intensity fluctuations, and RTP activation and quenching. This system pioneered reversible long-wavelength red RTP regulation in CDs composites, effectively coupling a photoinduced fluorescence color change with the control of yellow RTP (Fig. 10b). TPVBA-CD photochromism stems from molecular photoisomerization, whereas RTP reversibility is correlated with UV-generated singlet oxygen from molecular oxygen and the spatial confinement effect of the PMMA matrix.

4.2.2 Photochromic molecules and energy transfer. Energy transfer regulation is another important mechanism for achieving dynamic fluorescence color changes in CDs. This approach typically involves introducing photochromic molecules such as SP and diarylethene (DT). Under ultraviolet irradiation, these molecules undergo structural transformations between open-ring and closed-ring forms, accompanied by significant absorption spectral changes. CD-conjugated photochromic molecules mainly use SP and DT. For SP specifically, UV irradiation cleaves the C–O bond in SP, converting it from a colorless closed-ring state to a blue/purple open-ring MC form. This structural change causes a characteristic absorption redshift to approximately 550 nm. When the closed-ring form's absorption band overlaps with the CDs' emission spectrum, FRET conditions are established, enabling fluorescence color modulation to red. This process is reversible under visible light or thermal stimulation, where the molecule returns to its original closed-ring configuration. DT exhibits distinct photochromic behavior. UV irradiation triggers their open-ring isomers to undergo *cis–trans* isomerization through double-bond reorganization, converting them to closed-ring isomers with a corresponding blueshift in the absorption spectrum. Conversely, visible light irradiation reverses this process, restoring the open-ring form through a reversible photoisomerization accompanied by absorption redshift and color fading.

A seminal study by Ma *et al.*[153] demonstrated this principle *via* solvothermally synthesized CDs surface-modified with DT.

Under UV light, DT transitioned to its closed-ring form, with an absorption peak at 554 nm overlapping the CDs' green emission (525 nm). This induced FRET-mediated fluorescence quenching, reducing the QY from 12.9% to 0.6% with 95.3% modulation efficiency. Remarkably, the fluorescence switching exhibited stable reversibility over 6 cycles of alternating UV/visible light irradiation (Fig. 11a). In addition, Wang *et al.* further advanced this approach by covalently conjugating CDs with DT and embedding them in a PMMA matrix. Closed-ring DT increased π–π stacking and nonradiative decay, achieving 96.3% modulation efficiency. The film displayed a reversible color shift from light yellow to violet under UV light, accompanied by fluorescence attenuation. The emission intensity remained nearly unchanged after 3 cycles of UV/vis irradiation, underscoring its robustness for solid-state applications.[154] SP, another widely used photochromic molecule, offers complementary advantages. Jin *et al.*[54] engineered nitrogen-doped CDs encapsulated within a cellulose derivative (C–Im^+–SP) containing imidazolium and SP groups. UV irradiation opened the SP ring to the MC state. MC's 620 nm absorption overlapped with the NCDs' 467 nm blue emission, activating FRET (Fig. 11b). This reduced the blue fluorescence intensity by 60% while enhancing red emission fourfold, with over 95% reversibility under visible light. For the solid-state films, a photochromic shift from blue to red was observed. To address the aggregation-induced quenching of SP in solids, Zhu *et al.*[155] covalently anchored CDs onto amino-modified porous SiO_2 nanoparticles, followed by physical adsorption of SP (SP@SiO_2–CDs). The porous SiO_2 matrix provided spatial freedom for SP isomerization, enabling UV-triggered FRET from the blue fluorescence of the CDs to MC-SP, which resulted in a 60% decrease in blue emission and a fourfold increase in red emission, which was steadily switched by alternating UV and white light irradiation and can be repeated at least 10 times. By further design, Zhu *et al.*[156] grafted CDs onto aminated TiO_2–NH_2 surfaces *via* a silane coupling agent, forming TiO_2–CD composites, followed by loading SP into the pores through solvent adsorption. The synthetic strategy modulates the pore structure to enable spatial freedom for SP isomerization while achieving stable CDs to TiO_2–NH_2 binding *via* amidation reactions. The principle is based on the reversible isomerization of SP under UV/white light irradiation and its FRET effect with the CDs: UV light induces the conversion of SP to MC. The absorption spectrum of MC overlaps with that of the CDs, triggering FRET to reduce the blue fluorescence of the CDs while enhancing the red fluorescence of MC; white light irradiation reverses the isomerization and shuts down FRET, and the system retains color-fading properties after 10 cycles (Fig. 11c). The photochromic property of a material directly affects its optical properties, as the color of the material changes from light yellow to purple under UV light irradiation, the fluorescence changes from blue to red, and the fluorescence intensity changes dynamically with MC aggregation. For supramolecular assembly, Wu *et al.*[30] first

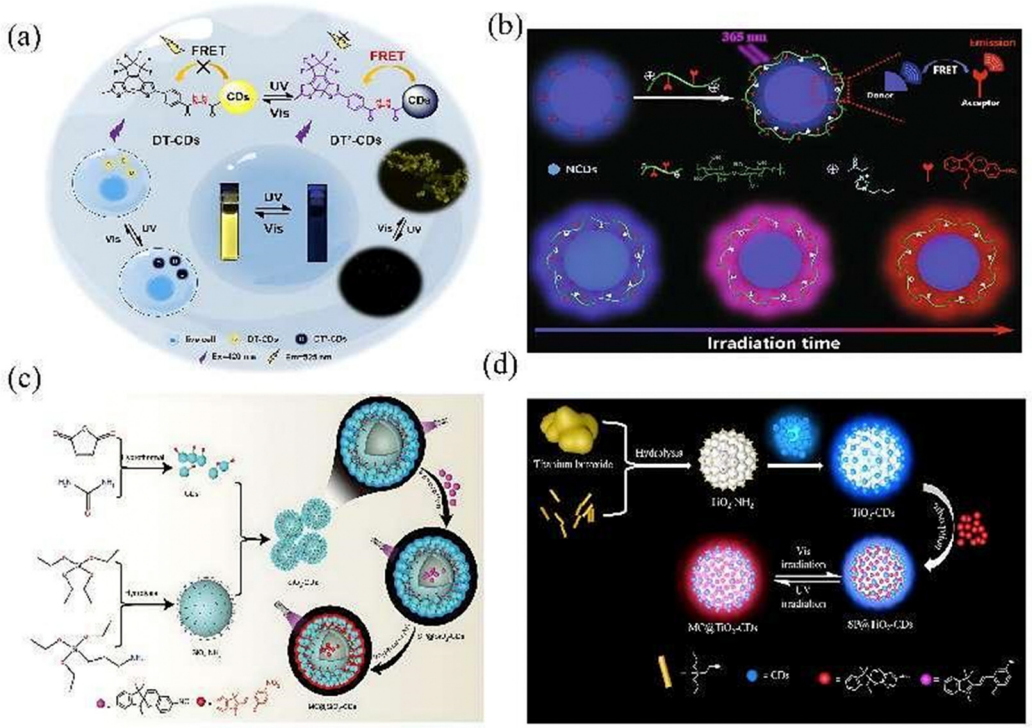

Fig. 11 (a) UV/vis light-regulated CDs-DT fluorescence switching *via* FRET quenching and visible-light recovery. Reproduced with permission.[153] Copyright 2023, Springer Nature. (b) FRET-mediated dynamic fluorescence modulation in cellulose-encapsulated NCDs *via* SP isomerization. Reproduced with permission.[54] Copyright 2021, Elsevier. (c) Supramolecular nanofiber assembly for tunable energy transfer. Reproduced with permission.[156] Copyright 2019, American Chemical Society. (d) TiO_2–CDs/SP hybrid system with pore-modulated isomerization. Reproduced with permission.[30] Copyright 2024, Science China Press.

synthesized the functionalized CDs by pyrolyzing a mixture of CA and diethylenetriamine and then amidating it with succinic anhydride. These CDs were then self-assembled with a styrylpyridinium-modified diarylvinyl derivative (12^+) and melon rings in water to form supramolecular nanofibers. The cavity structure of the guar ring effectively immobilized the conformation of the 12^+ molecule, limiting the rotation of the C=C double bond and significantly enhancing its fluorescence intensity (the emission peak redshifted from 560 to 582 nm). Further incorporation of CDs into supramolecular nanofibers to construct ternary assemblies revealed that UV irradiation transformed the 12^+ molecule from an open-loop form (OF-12^+) to a closed-loop form (CF-12^+), disrupting the conjugated system and reducing the fluorescence intensity to 23% of its original value. Visible light irradiation reversibly shifts the closed-loop form back to the open-loop form, with a fluorescence recovery of up to 97% (Fig. 11d). This process controls the energy transfer efficiency by regulating the molecular energy levels: in the open-loop state, FRET between CDs and 12^+ is enhanced; in the closed-loop state, the FRET pathway is blocked, and the system exhibits mainly the intrinsic fluorescence of CDs.

4.2.3 Other strategies. In addition to the two main photochromic mechanisms mentioned above, the photochromic properties of CDs can also be dynamically regulated through a multicomponent synergistic composite strategy. By compositing CDs with functional materials such as polymers, inorganic nanomaterials or supramolecular systems, the photochromic efficiency can be significantly enhanced by utilizing physical interactions or chemical coupling between components. For example, Wu *et al.*[56] prepared a CDs solution *via* a hydrothermal method and subsequently anchored the CDs onto a porous TiO_2 thin film to form a CDs/TiO_2 nanocomposite film. Under blue light irradiation, the films prepared by drop-casting anchoring (DA) and immersion anchoring (IA) exhibited bidirectional photochromic behavior. In the DA–CDs/TiO_2 film, the CDs were excited under visible light, but their limited contact with TiO_2 hindered electron transfer, leading to localized heat accumulation and carbonization, which increased the carbon content and darkened the film. Conversely, in the IA–CDs/TiO_2 film, the CDs were fully anchored within the TiO_2 pores, and the photoexcited electron–hole pairs induced oxidation reactions that resulted in photobleaching and a lighter film color. Wan *et al.*[157] introduced GQDs into an organic/inorganic hybrid system to fabricate rewritable paper with superhydrophobic and photochromic properties. Under UV irradiation, this material exhibited a rapid response and high-contrast photochromic characteristics—with a maximum color contrast reaching 61.92% and 86.8% of the maximum contrast achieved within 10 s. This effect was attributed to the GQDs promoting electron transfer from a donor (AMT) to an acceptor (PVP) under UV light, thereby accelerating the photochromic reaction. Specifically, under light excitation, the W^{6+} in AMT is reduced to W^{5+}, generating indigo blue and inducing a color change, whereas in the presence of air, W^{5+} is oxidized back to W^{6+}, allowing spontaneous fading.

Mogharbel *et al.*[52] developed a self-healing anticounterfeiting ink by embedding NCDs into a carboxymethyl cellulose (CMC) hydrogel, which formed an NCDs@CMC composite ink. Under UV irradiation, the ink exhibited pronounced photochromic behavior, changing from colorless to blue. This phenomenon originated from UV-induced electron excitation from the NCD valence band to the conduction band, generating electron–hole pairs that trigger redox reactions on the NCD surface, leading to fluorescence emission. In another study, Zhong *et al.*[27] synthesized a CMC-based smart-responsive hydrogel (CCA) by a hydrothermal method, combining CDs as fluorescent elements with photochromic ammonium molybdate (Mo) to form a composite material with a three-dimensional chemically crosslinked network structure, which realizes the dual reversible switching functions of fluorescence and photochromism. The core principle of photochromism is that Mo^{6+} in ammonium molybdate is partially reduced to Mo^{5+} through CT induced by UV light, which leads to internal electron transfer and triggers a color change, resulting in the rapid transformation of the material from a light yellow color to a dark green color. Zhang *et al.*[29] proposed a visible-light-responsive system of boron-doped CDs embedded *in situ* in a phenylboronic acid-derived polymer matrix *via* a two-step thermal treatment. Visible light triggered dynamic B–B and C–O–B crosslinking between the boron-doped CDs and the polymer, which increased the matrix rigidity to stabilize the triplet excitons, prolonged the RTP lifetime from 2.53 ms to 0.72 s, and increased the RTP intensity by a factor of 5.91. Sun *et al.*[158] used a one-step solvothermal method to synthesize sodium-doped CQDs and the byproduct 4,4′-diaminoazobenzene. Sodium doping regulates the surface energy level of the CQDs through the construction of the CQDs–O–Na^+ structure, while photoisomerization of the byproduct leads to red-shifting of the absorption spectrum from 400 to 500 nm, which triggers an internal filtration effect by overlapping the fluorescent spectrum of the dots and results in a reversible color shift of the material from yellow to orange in the ultraviolet region color shift under UV light. In addition, hydrogen ions induce a shift in the fluorescence emission wavelength of the CDs, and the optical dynamics of the attenuation and color switching result from the synergistic effect of photoisomerization and energy transfer. These studies systematically revealed the mechanisms of the doping strategy, dynamic cross-linking, and synergistic effects of byproducts on the optical behavior of photochromic CDs through differentiated design, providing new ideas for the development of multifunctional dynamic optical materials.

We summarize in Table 2 the photochromic properties of a variety of photochromic CD composites reported in recent years and their mechanisms of discoloration.

5. Applications of photoresponsive carbon dots

5.1 Bioimaging and biomedicine

Due to their advantages of small size, fluorescent properties, low toxicity and biocompatibility, photoresponsive CDs have important applications in bioimaging and biomedicine. Recent

Table 2 Color changes and factors of photochromic CD-based materials under different excitations

Material name	Medium	Excitation wavelength	Color change	Reversibility	Mechanism	Ref.
PSPxCD	Polyurethane elastomer	418 nm	Colorless/light yellow to purple	Reversible under white light exposure	SP photoisomerization	159
GQDs-amine	Transparent film	365 nm	Blue/green to red	Reversible under visible light	FRET between GQDs and SP	160
CDs/TiO_2	Nanocomposite	365 nm	Blue to colorless	Oxygen recovery (20 min)	TiO_2 photocatalytic redox reaction with CDs as electron mediators	161
CD-to-MC	Polymer nanoparticles	365 nm	Blue to green to red	Reversible *via* UV/visible light switching	SP isomerization and FRET	162
SP-CDs	Solution/solid	365 nm	Colorless/blue to deep purple/red	Light or pH adjustment	SP photoisomerization and protonation	163
TiO_2–CDs	Solid composite	365 nm	Blue to pink to red	White light exposure	Dynamic FRET between CDs and SP	156
NCDs@C–Im^+–SP	Solid coating/ink	365 nm	Blue fluorescence to red fluorescence	Visible light exposure	Cellulose-SP photoisomerization and FRET	54
SP@SiO_2–CDs	Flexible film	365 nm	Yellow to pink	White light exposure	Dual-channel FRET between SiO_2–CDs and SP	155
B-CDs@pPBA	Solid film	400–500 nm	Phosphorescence lifetime: 0.72 s to 2.53 ms	Reversible upon light cessation	Light-induced crosslinking between B-CDs and polymer	29
CDs@DETN	Solution/solid	365 nm	Cyan to orange-red (fluorescence); pale yellow to purple (solution)	Spontaneous recovery	Radical changes on CDs surface	152
GQDs	Super-hydrophobic film	395 nm	White to blue	Heat or visible light exposure	Charge transfer in graphene quantum dots	157
Py-CDs@PMMA	Solid composite film	365 nm	Blue fluorescence to red RTP	Air exposure (10 min)	Pyrene's large conjugation and PMMA matrix rigidity	28
TPVBA-CDs@PMMA	Solid composite film	365 nm	Cyan fluorescence to blue fluorescence (enhanced RTP)	Oxygen-regulated ($^3O_2 \leftrightarrow {}^1O_2$ conversion)	Tetraphenylethylene photocyclization	28
CDs/PVP	Flexible film	400 nm	Transparent to grayscale phosphorescence	Oxygen-dependent recovery	Halogen doping enhances ISC	164
DT–CDs	Solid	254 nm	Light gray to purple	Reversible under visible light	DT closed-ring form acts as FRET acceptor	154
CDs–PVP	Solid film	365 nm	Blue to yellow	Oxygen regulation or light exposure	NI radical generation and oxygen quenching	31
CMC/CDs/CCA hydrogel	Hydrogel	365 nm	Light yellow to green	Ethanol treatment or heat (60 °C)	Ammonium molybdate photoredox reaction	27

advances in synthesis strategies have enabled multifunctional CDs systems for cell imaging, tumor therapy, and antibacterial applications.

In the field of bioimaging, Wen and colleagues converted chlorophyll derivatives into hydrophobic CDs *via* a microwave-assisted method, obtaining an NIR fluorescent material with a maximum emission peak at 680 nm. Water-soluble CDs assemblies, formed by self-assembly with DSPE-mPEG2000, exhibited strong fluorescence emission in the NIR region, successfully enabling deep tissue imaging. The material maintained excellent fluorescence stability in 4T1 cells, preserving >90% of the cell viability at 250 μg mL^{-1}.[165] *In vivo* experiments revealed no significant changes in body weight in the mice, confirming its biosafety. In tumor therapy, the carbon dot system, when excited by a 671 nm laser, exhibited a singlet oxygen QY of 0.62. *In vitro* experiments effectively killed 4T1 tumor cells, whereas *in vivo* studies demonstrated significant tumor growth inhibition through tumor-targeted accumulation, highlighting its potential for photodynamic therapy. Wu and colleagues developed F- and N- codoped CDs that generate $^{\bullet}OH$ and $^{\bullet}O_2^-$ *via* type I photoreactions, overcoming the oxygen dependence typical of traditional type II photodynamic therapy.[166] These CDs showed significant therapeutic effects in hypoxic HepG2 cells and 3D multicellular spheroid models, and with a green PLQY of 18.25%, they enable real-time monitoring of the treatment process. For antibacterial applications, Jiang *et al.*[167] prepared P-CDs that exhibit oxidase-like activity under light irradiation, generating O_2^- radicals. The inhibitory effects on *Escherichia coli* and *Staphylococcus aureus* were found to be positively correlated with both concentration and light exposure time. Even at a concentration of 160 μg mL^{-1}, the material maintained a cell viability above 80%, demonstrating good biocompatibility. Additionally, Lee and colleagues designed a hyaluronidase-responsive CDs gel system that triggers the targeted release of CDs in response to the bacterial microenvironment.[168] When combined with white light-induced $^1O_2$ generation, this system effectively eliminates drug-resistant bacteria while enabling dynamic monitoring of wound healing. To address complex therapeutic requirements, Yan and colleagues constructed a CDs/TiCN heterojunction nanozyme that exhibits mild photothermal effects (43 °C) and sonodynamic properties within the NIR-II window (1000–1350 nm). The enhanced charge carrier separation efficiency in the heterojunction synergistically improves the catalytic activity and generation of reactive oxygen species (ROS), offering a multimodal solution for deep-seated tumor therapy.

Current research trends indicate that photoreceptive CDs are evolving from single-function systems to integrated theranostic

platforms.[38] Future studies should focus on extending their optical absorption into the NIR-II region, optimizing the ROS QY, and systematically evaluating their metabolic pathways and long-term biosafety in complex biological environments to accelerate clinical translation.

5.2 Fluorescence detection

Photoresponsive CDs have unique advantages in areas such as environmental monitoring because of their surface-rich functional groups and ability to be further modified. In recent years, researchers have designed and optimized synthetic and functionalization strategies for CDs, developing various high-performance fluorescent probes for detecting specific substances in environmental and biological samples. Xu *et al.*[169] reported a dual-ratiometric fluorescent probe based on PEG-passivated CDs for highly sensitive detection of H_2S. Under 270 nm excitation, the CDs exhibited both ultraviolet and green emission, whereas under 365 nm excitation, only green emission was observed. Upon the addition of Na_2S, the ultraviolet emission gradually decreased, the green emission slightly increased, and a new blue emission emerged, the intensity of which increased linearly with the Na_2S concentration. Dual-ratio analysis (F_{455}/F_{350} and F_{455}/F_{523}) enabled H_2S detection with a 7.0 nM limit across 0–800 μM, demonstrating exceptionally high sensitivity and a broad detection range. Moreover, this probe successfully detected H_2S in living cells, confirming its applicability in biological environments. Zhang *et al.*[170] developed a mixed sensor by integrating Se, N-doped blue/yellow emissive CDs with curcumin for turn-on fluorescence detection of F^-. The CDs synthesized *via* a hydrothermal method exhibited blue emission and yellow emission. Curcumin significantly quenched the yellow fluorescence of the CDs *via* IFE. Upon the addition of F^-, curcumin forms a complex with F^-, inducing a blueshift in its absorption band and weakening the IFE, thereby restoring yellow fluorescence and enabling F^- detection. The detection limit was determined to be 0.39 μM—well below the World Health Organization's maximum allowable concentration of 52.6 μM for F^- in drinking water—and the sensor exhibited excellent accuracy and reliability in tap water and milk samples. The photoresponsive oxidase-like activity of CDs has provided a new approach for enzyme-free photoelectrochemical detection. Li *et al.*[171] developed a CD-based nanozyme whose photocatalytic activity originates from light-induced ICT that generates hydroxyl radicals ($^{\bullet}OH$). Under illumination, the CDs catalyze the oxidation of the chromogenic substrate 3,3′,5,5′-tetramethylbenzidine (TMB) by dissolved oxygen to produce a blue oxidized product (oxTMB), while antioxidants inhibit the colorimetric reaction by scavenging $^{\bullet}OH$. This light-responsive catalytic mechanism is directly translatable into photocurrent changes, laying the groundwork for the development of photoelectrochemical sensors that operate without H_2O_2. Similarly, Yang *et al.*[172] employed the photoresponsive oxidase-like activity of CDs/g-C_3N_4 composites to catalyze TMB oxidation under visible light, achieving detection through the inhibitory effect of carbofuran hydrolysis products (detection limit: 2.52 μM). Moreover, CDs serve as excellent photosensitizers that enhance catalytic performance in photoelectrochemical detection. For example, Yuan *et al.*[173] constructed a CDs/B-TiO_2 composite photoelectrode by loading CDs onto branched TiO_2 (B-TiO_2) *via* a hydrothermal method. The CDs not only extended the visible light absorption range of TiO_2 but also suppressed the recombination of photogenerated electron–hole pairs through interfacial electron transfer. Under visible light, photoexcited electrons from the CDs were injected into the conduction band of TiO_2, forming a stable photocurrent. Moreover, H_2O_2 produced by the catalytic action of glucose oxidase consumes electrons, leading to a decrease in the photocurrent signal and enabling the sensitive detection of glucose (detection limit: 0.043 mM).

In summary, photoresponsive CDs exhibit outstanding performance in photoelectrochemical detection, particularly in the highly sensitive and selective detection of specific analytes. By optimizing the synthesis and functionalization of CDs and integrating various detection mechanisms—such as the IFE and dual-ratiometric analysis—carbon dot fluorescent probes have great promise for applications in environmental monitoring, food safety, and biomedical diagnostics. With further advancements in understanding the fluorescence mechanisms and synthesis technologies of CDs, their applications in photoelectrochemical detection are expected to become even more extensive and in depth, offering novel solutions to practical challenges.

5.3 Anti-counterfeiting and encryption

The application of light-responsive CDs in anticounterfeiting encryption technology is mainly attributed to their tunable optical properties, multiple response mechanisms, and advantages of low cost and environmental friendliness. Yang *et al.*[174] synthesized NCDs *via* a hydrothermal method using *p*-PDA and urea as precursors. They then obtained g-C_3N_4 powder by calcining melamine, followed by grinding, and finally prepared NCDs@g-C_3N_4 composites through high-temperature stirring. When g-C_3N_4, NCDs, and NCDs@g-C_3N_4 are mixed with water at 1.2 wt% to prepare fluorescent inks, they exhibit white, red, and gray colors under visible light, respectively, and bright blue, orange, and cyan fluorescence under 365 nm UV light (Fig. 12a). The clear, intense, and bright effects under UV irradiation enable high-efficiency encryption and anticounterfeiting, regardless of whether the materials are used individually or in combination.

Furthermore, CDs can be synthesized from a wide range of precursors *via* simple methods, and their nontoxic and eco-friendly nature makes them suitable for large-scale production of low-cost anticounterfeiting inks or films.[178] When these materials are combined with other materials, their stability can be enhanced, or their multifunctionality can be integrated. Their nanoscale size facilitates high-precision patterning and dynamic responses, further increasing the difficulty of counterfeiting. For instance, Tian *et al.*[175] employed a microwave-assisted method using CA and ammonia to synthesize CD-1 and obtained CD-2 by heating under a nitrogen atmosphere at 200 °C. By dissolving CD-1 or CD-2 powders in a polyvinyl alcohol (PVA) aqueous solution and spin-coating them onto quartz plates, followed by annealing at different temperatures, CD-1@PVA and CD-2@PVA composites were prepared. The different annealing temperatures induced variations in the oxygen content, thereby affecting

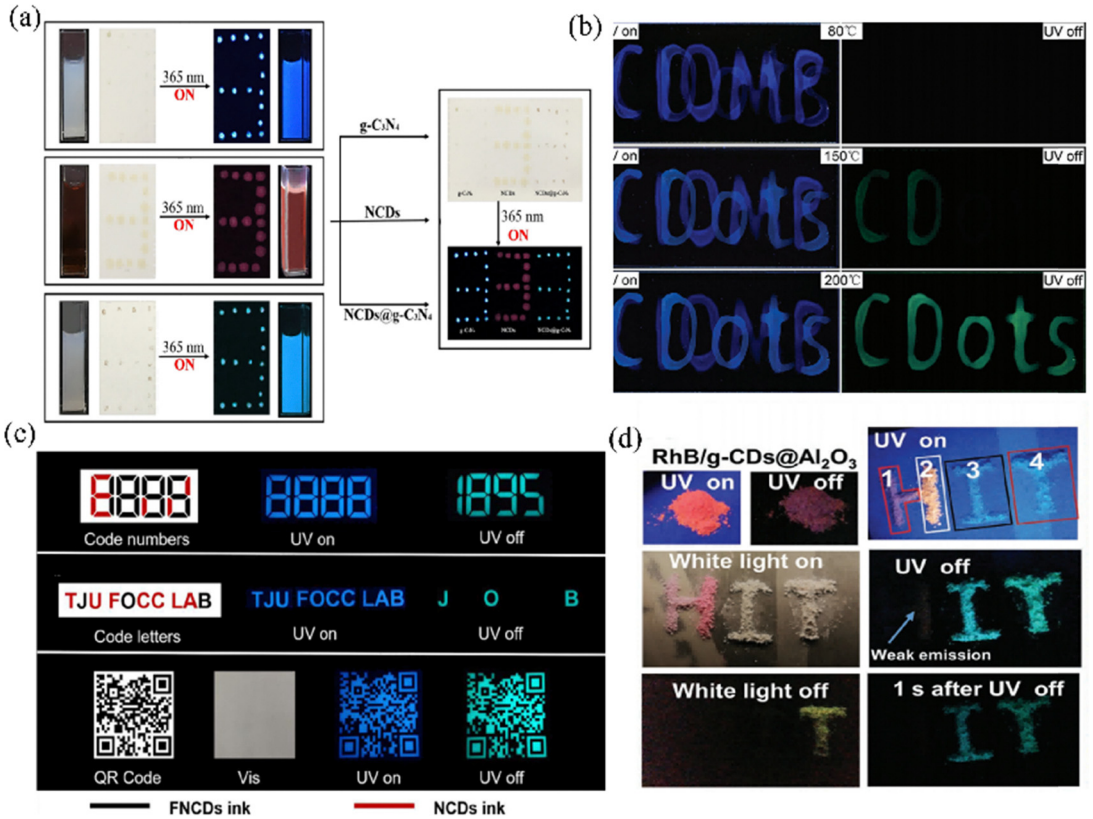

Fig. 12 (a) NCDs@g-C_3N_4 composite fluorescent inks for dual-mode anti-counterfeiting. Reproduced with permission.[174] Copyright 2019, Elsevier. (b) Multi-level encryption *via* annealing-controlled phosphorescence in CD/PVA composites. Reproduced with permission.[175] Copyright 2018, Wiley-VCH. (c) pH-stable FNCDs inks with self-protected RTP. Reproduced with permission.[176] Copyright 2021, Elsevier. (d) FRET-enabled multi-channel encryption with g-CDs@Al_2O_3/RhB. Reproduced with permission.[177] Copyright 2023, Wiley-VCH.

the fluorescence and RTP properties to achieve multilevel data encryption. Specifically, when three composites—blue fluorescent citrazinic acid (CzA@PVA), CD-1@PVA, and CD-2@PVA—were used, annealing below 80 °C produced only an indistinguishable blue fluorescent pattern. Upon annealing at 150 °C, the characteristics of CD-2@PVA exhibited green RTP, decoding the first level of encrypted information; at 200 °C, both CD-1@PVA and CD-2@PVA presented green RTP, whereas the CzA@PVA fluorescence signal weakened, thereby decoding the second level of encrypted information (Fig. 12b).

The fluorescence and RTP properties of CDs can be tuned to exhibit multiple colors through size control, surface modification, or elemental doping. Liu *et al.*[176] dissolved fructose and diethylenetriamine (DETA) in ethanol and performed a solvothermal reaction at 180 °C to synthesize NCDs. These samples were subsequently placed in a nickel reactor and subjected to a gaseous fluorination reaction under a 3% F_2/N_2 atmosphere, yielding FNCDs. FNCD inks exhibit stable fluorescence under various pH conditions, making them suitable for secure printing and anticounterfeiting. Moreover, when coated on paper, the FNCDs demonstrate self-protected RTP stability under oxygen-free conditions, retaining 87.3% of their RTP intensity under 328 nm irradiation. Although both the FNCDs and NCDs emit blue fluorescence in aqueous solution, the FNCDs also display RTP under UV light, endowing them with unique emission properties in both the visible and UV regions (Fig. 12c). This makes them highly advantageous for encoding complex pattern information and anticounterfeiting. Zhang *et al.*[179] synthesized yellow, orange, and red fluorescent CDs (Y-CDs, O-CDs, and R-CDs) within 7 minutes *via* a microwave-assisted method, with *o*-PD as the carbon and nitrogen source, BA as the boron source, and potassium chloride as the catalyst. The codoping of boron and nitrogen induced redshifted fluorescence by modulating the surface defect states and energy-level structure of the CDs. The O-CDs and R-CDs exhibited dual-peak fluorescence characteristics due to the synergistic effects between the carbon core and surface defects, and by adjusting the precursor ratio, the fluorescence color could be precisely tuned from yellow to red. In encryption applications, R-CDs and Y-CDs can represent binary codes "0" and "1", respectively. By printing a fluorescent binary array on filter paper, for example, the code "01010001" can be decoded as "QDU" under UV light. Inherent invisibility and multilayer encryption mechanisms enhance information security.

The optical response of CDs can be dynamically modulated by external stimuli including light, solvents, and temperature. For example, solvent-responsive CDs display different colors in water *versus* organic solvents, photoresponsive materials can exhibit layered encrypted information under specific UV light, and lifetime-tunable systems may require time-resolved equipment for decoding. Li *et al.*[177] synthesized CDs *via* one-pot

hydrothermal treatment of lily alkaloids at 200 °C for 2 h and then blended them with BA at various concentrations through thermal fusion to obtain G-CDs@BA, Y-CDs@BA, R-CDs@BA, and NIR-CDs@BA composites. An increase in the carbon dot content within BA enhanced aggregation, leading to significant electronic interactions that caused energy level splitting to form low-energy aggregated states. This resulted in a continuous shift in the RTP color from 530 to 555, 585, 625, 645, and 750 nm. Upon the spraying of methanol on G-CDs@BA, the methanol molecules disrupted the hydrogen bonds within BA, weakening the interaction between the CDs and the matrix. The loss of the BA passivation effect resulted in closer aggregation of CDs and enhanced electronic interactions, leading to energy level splitting into low-energy states. Consequently, the RTP color of G-CDs@BA shifted from green to red, and the fluorescence color changed from green to yellow. This responsive behavior suggests potential applications in high-security anticounterfeiting labels or dynamic information encryption (Fig. 12d). Collectively, these properties make CDs an ideal material for anticounterfeiting encryption applications, offering a combination of flexibility, security, and sustainability.

5.4 Photocatalysis

The key advantages of CDs as photocatalytic materials stem from their unique structural characteristics and functional design ability. Their broad spectral absorption (UV to NIR) and tunable bandgap (*via* elemental doping or surface modification) enable them to efficiently capture light energy and drive photocatalytic reactions.[180–182] Moreover, the abundance of surface functional groups (*e.g.*, hydroxyl and amino groups) and defect sites not only provides numerous active centers but also suppresses the recombination of photogenerated charge carriers through CT, thereby significantly increasing quantum efficiency. In addition, the environmentally friendly (biodegradability and low toxicity) and low cost (due to natural precursors) of CDs offer great prospects in water splitting, CO_2 reduction, and pollutant degradation.[41,183]

In photocatalysis, CDs have been utilized for the degradation of organic pollutants and water splitting. For example, Li *et al.*[184] prepared a three-dimensional ordered macroporous (3DOM) composite of CDs and bidoped TiO_2 for the efficient photocatalytic degradation of organic pollutants. In this composite, the electron extraction ability of the CDs, coupled with the light scattering effect of the 3DOM structure, significantly enhanced the photocatalytic performance—achieving a 92.7% degradation rate of phenol within 2 hours and a 96.4% degradation rate of rhodamine B (RhB) within 40 minutes under full-spectrum irradiation. Zhang *et al.*[181] explored the application of metal-free chiral CDs in the photocatalytic oxidation of DOPA. Due to their size-dependent bandgaps and photoresponsive properties, these CDs maintained high catalytic activity and selectivity at low temperatures, primarily because of their ability to reduce oxygen to generate superoxide anions *via* photogenerated electrons.

In electrocatalysis, CDs have been applied to both the hydrogen evolution reaction (HER) and the oxygen reduction reaction (ORR). Wu *et al.*[185] investigated the carbon dot-enhanced electrocatalytic HER by combining CDs with metal phosphides (*e.g.*, MoP). The high conductivity of the CDs and the strong metal–carbon interactions significantly improved the efficiency of the HER. The incorporation of CDs not only increased the overall conductivity of the electrocatalyst but also improved its activity by generating carbon vacancies and reducing the coordination number of the active sites. Zhou *et al.*[41] achieved efficient photoinduced atom transfer radical polymerization (photoATRP) by coupling SiCDs with a copper catalyst. These SiCDs, which exhibited PLQYs ranging from 11.2% to 75.6%, benefited from a reduced bandgap and increased nonradiative recombination rate, which significantly increased the photocatalytic efficiency. Additionally, Filippini *et al.*[183] studied covalent catalysis in aqueous media by employing amine-rich NCDs. These NCDs efficiently catalyzed various aminocatalytic carbonylation reactions *via* the formation of iminium and enamine intermediates, achieving high catalytic activity and selectivity with yields of up to 96% and complete enantioselectivity. Hu *et al.*[180] combined CDs with Ag_3PO_4 to accomplish the efficient photocatalytic reduction of 4-nitrophenol (4-NP). Here, the inclusion of CDs not only enhanced the light absorption of the photocatalyst but also, by forming heterojunction structures, markedly improved the separation and transfer efficiency of the photogenerated charge carriers.

In summary, light-responsive CDs have extensive application potential in catalysis. By tuning their size, doping elements, and surface functional groups, the photocatalytic and electrocatalytic performance of CDs can be significantly enhanced. These carbon dot-based catalysts have demonstrated excellent performance in the degradation of organic pollutants, water splitting, the HER, and the ORR, offering new insights and methodologies for the development of efficient and environmentally friendly catalysts.

5.5 LED emission

Due to their tunable fluorescence emission properties, CDs exhibit unique application value in the LED field. By precisely controlling the size distribution, surface functional group modifications, and elemental doping of CDs, it is possible to continuously cover emission wavelengths from blue to NIR. This capability provides key technological support for designing multicolor display devices and developing full-spectrum LEDs.[186] In terms of device fabrication, CDs can either serve directly as the core electroluminescent layer or be integrated with a polymer matrix to form hybrid materials that significantly increase emission efficiency *via* energy transfer effects.[187,188] Compared with conventional heavy metal-containing CDs, CDs offer the advantages of abundant precursor sources, simple synthesis procedures, and environmental friendliness, thereby substantially reducing both the manufacturing costs and the ecological risks associated with LED devices.[189]

In recent years, significant progress has been made in optimizing key performance parameters of carbon dot-based LEDs, particularly in the areas of red and NIR emission, solid-state luminescence performance, and dynamic white light color temperature tuning. Red and NIR-emitting CDs are critical for achieving full-color displays and bioimaging. For example,

Ji *et al.*[190] achieved large-scale synthesis of NIR-CDs derived from *o*-PDA *via* a microwave-assisted hydrothermal method, with a cost of only USD 0.1 per gram and a yield exceeding 96%. The fluorescence emission wavelength of these CDs can be reversibly tuned *via* a protonation–deprotonation process (red-shift of 47 nm), which increases the QY threefold. These NIR-CDs have been successfully applied as red fluorescent phosphors in LED devices, overcoming the challenges of scalable production for red-emitting CDs (Fig. 13a). In a 2023 study, Chen *et al.*[191] extracted CDs from green plants and, by designing a host based on active complexation to suppress aggregation-induced quenching, developed deep-red CDs with ultranarrow bandwidths (FWHM = 21 nm) and high QYs (>50%) at 673 nm. The LED fabricated with these CDs exhibited color coordinates of (0.692, 0.307), marking the first realization of high-color-purity deep-red carbon dot LEDs and advancing full-color display technology (Fig. 13b).

With respect to the optimization of solid-state luminescence, Xu *et al.*[192] proposed a surface polymer chain modification strategy to suppress π–π stacking effects, thereby fabricating highly efficient solid-state luminescent CDs with emission ranging from visible to NIR (570–721 nm) and a maximum QY of up to 67.7%. They further constructed white LEDs and plant growth LEDs with adjustable color temperatures ranging from 1882 to 5019 K, with the latter showing improved performance in enhancing plant photosynthetic efficiency compared with traditional light sources (Fig. 13c). Zhao *et al.*[195] utilized the non-planar structure of triphenylamine derivatives to inhibit carbon core aggregation, and orange (595 nm) and yellow (575 nm) solid-state luminescent CDs were developed. Their single-layer LED devices achieved a maximum brightness of 9450 cd m^{-2} and a current efficiency between 1.57 and 2.34 cd A^{-1}, positioning their performance among the best of similar devices.

Dynamic color temperature tuning of white LEDs is a core requirement in lighting applications. Sun *et al.*[193] encapsulated multicolor CDs (blue, green, red, and NIR) with boron oxide (B_2O_3) to achieve afterglow emission wavelength tunability (463–722 nm), constructing white LEDs with CIE coordinates of (0.32, 0.34) and a color rendering index of 81.1. The long afterglow characteristics effectively suppressed the zero-cross flicker in AC-powered LEDs (Fig. 13d). Wang *et al.*[194] proposed a strategy based on the aggregation-induced redshift effect, whereby controlling the aggregation degree of CDs enabled continuous tuning of the color temperature of white LEDs (from 2863 to 11 240 K).

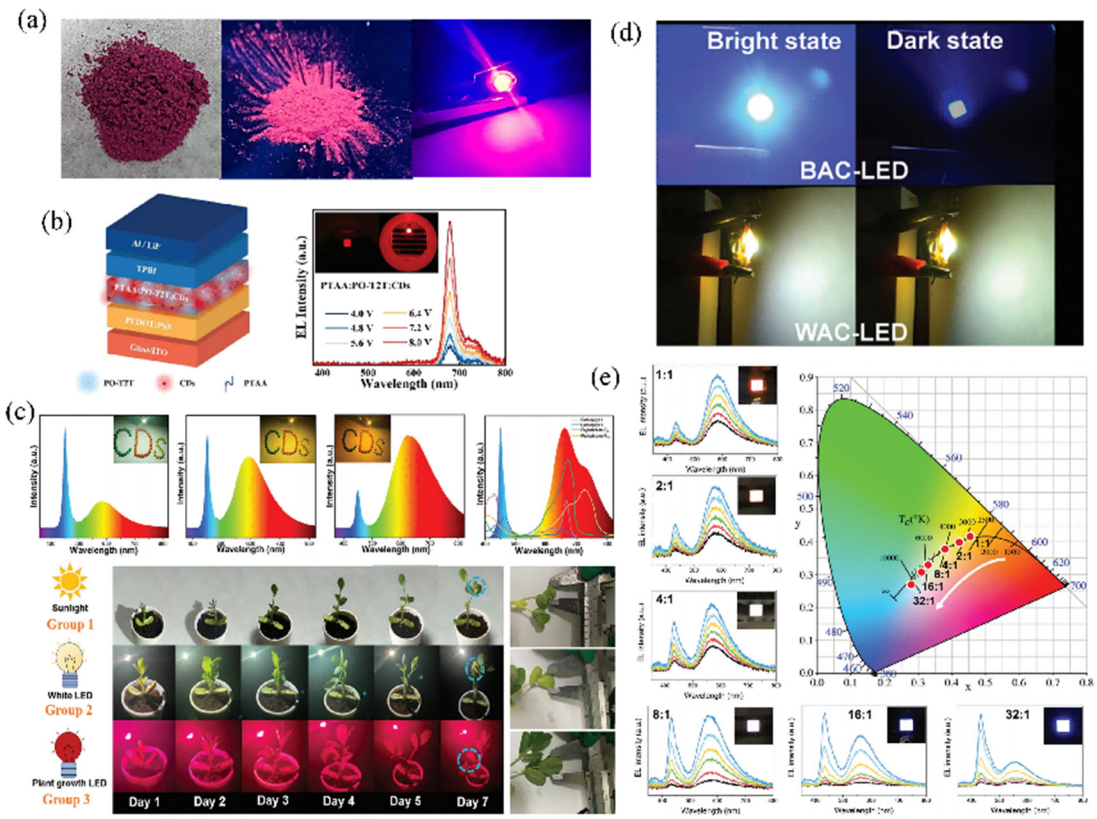

Fig. 13 (a) NIR-CDs as red phosphors. Microwave-synthesized CDs emit red light under UV, integrated with blue LED chips for red LEDs. Reproduced with permission.[190] Copyright 2022, Elsevier Ltd. (b) Deep-red CDs for high-purity LEDs. Plant-derived CDs enable ultra-narrow deep-red electroluminescence, advancing display technology. Reproduced with permission.[191] Copyright 2023, Wiley-VCH. (c) Multi-functional white LEDs. Tunable emission from visible to NIR supports general lighting and enhanced plant growth. Reproduced with permission.[192] Copyright 2022, Wiley-VCH. (d) Anti-flicker white LEDs. Afterglow CDs suppress flicker in AC-driven LEDs. Reproduced with permission.[193] Copyright 2024, Wiley-VCH. (e) Color-tunable white LEDs. Aggregation-controlled CDs adjust the color temperature from warm to cool white. Reproduced with permission.[194] Copyright 2021, Wiley-VCH.

Their devices achieved a maximum brightness of 4917 cd m^{-2} and an external quantum efficiency of 0.87%, offering new prospects for personalized lighting applications (Fig. 13e).

Due to their unique optical tunability, environmental friendliness, and low cost, they are gradually transitioning from laboratory research to practical applications and are poised to become core materials for next-generation green lighting and flexible display technologies.

5.6 Others

In addition to the several applications mentioned above, CDs have a wide range of potential applications in areas such as environmental remediation, energy storage and conversion, and smart materials.[196] In environmental remediation, CDs have been used to remove heavy metal ions from water, *e.g.*, Banerjee *et al.*[197] successfully removed Cd^{2+} ions from water by using CDs with a removal rate as high as 93.2% and realized the sustainable use of cadmium ions by transferring the Cd^{2+} ions from the aqueous phase to the organic phase through a phase transfer method. In addition, CDs have been used for air purification, and their photocatalytic properties can degrade volatile organic compounds and other pollutants in the air and improve air quality.

In the field of energy storage and conversion, CDs have been used to develop photocharged supercapacitors and lithium-metal batteries. Prishkolnik *et al.*[198] prepared a photocharged supercapacitor based on CDs and a temperature-sensitive polymer, where the CDs induced a hydrophilic–hydrophobic phase transition of the polymer under light irradiation and simultaneously acted as an electrolyte to increase the capacitance of the capacitor. Liu *et al.*[199] prepared a high-performance gel–polymer electrolyte for use in lithium batteries *via* CDs, which significantly improved the ionic conductivity and cycling stability of the batteries.

CDs can also be used as auxiliary or smart materials for related applications. Abbas *et al.*[200] reported for the first time an advanced oil-in-water (O/W) emulsion costabilized by a cationic surfactant and equally positively charged CDs. In this emulsion, cationic surfactant molecules adsorb at the oil–water interface, lowering the interfacial tension and imparting a positive charge to the oil droplets, thus ensuring strong electrostatic repulsion between them. Moreover, the cationic CDs are distributed in the aqueous phase, reducing water secretion and preventing oil droplet agglomeration and merging. The stability of this emulsion is universal for a wide range of oil phases, such as alkanes, aromatic hydrocarbons, and esters. Niu *et al.*[39] engineered a smart soil composite by integrating CDs with conventional soil, which is capable of automatically adjusting the porosity and size of agglomerates. This smart soil utilizes the moisture responsiveness of the CD-based material to increase the soil height to 150% in response to moisture stimulation, similar to the effect of earthworms on the soil structure. This smart soil is effective at preventing soil sloughing and promoting crop growth. For example, the growth rate of corn seedlings in smart soil was 40% greater than that in conventional soil. In addition, smart soil is environmentally friendly and biodegradable, indicating its significant potential for use in modern agricultural practices and sustainable agricultural development.

In addition to the several applications mentioned above, CDs have a wide range of applications in multiple fields on the basis of their tunable surface functional groups, photoresponsiveness and biocompatibility. In the medical field, CDs and PVA composites with photothermal conversion capabilities and rapid shape recovery can be used for medical scaffolds and flexible sensors.[201] In the field of metal corrosion protection, pectin-derived CDs exhibit corrosion inhibition efficiency through adsorption to form a film,[202] which may involve an electrochemical protection mechanism and help extend the service life of metal products. In the field of food packaging, mango peel CDs, for example, can effectively block ultraviolet rays and have fluorescent properties, thus enhancing the protective function of packaging films and helping to maintain the freshness and quality of food.[203] In smart packaging systems, polyaniline-functionalized CDs serve as freshness indicators *via* colorimetric responses, and when compounded with cellulose nanofibers, they are able to monitor pH and ammonia in real time, thus realizing the dual function of smart packaging films.[204] In addition, chlorogenic acid CDs embedded in fucoidan-based films can significantly reduce UV transmittance and impart antimicrobial properties to the coating, making it suitable for food packaging and outdoor protective materials.[205] The unique physicochemical properties of CDs enable multifunctional applications across diverse fields, including medicine, anticorrosion, food packaging and smart packaging, providing strong support for the development and innovation of related technologies.

6. Summary and prospects

This review systematically analyzes recent advances in photoresponsive CDs, with focus on classification frameworks, synthetic methodologies, and luminescence mechanisms. On the basis of their photoresponsive characteristics, CDs are primarily classified into two systems: photoluminescent and photochromic. Photoluminescence behavior is governed by intricate regulatory mechanisms involving carbon core emission, molecular state transitions, surface state effects, and CEE. Photochromic CDs rely on reversible processes such as energy transfer, radical generation, and molecular isomerization. Synthesis approaches for light-responsive CDs mainly fall into top-down methods (*e.g.*, laser ablation and chemical oxidation) and bottom-up strategies (*e.g.*, hydrothermal treatment, solvothermal synthesis, and microwave-assisted preparation). Precise optimization of the optical properties can be achieved through controlled modulation of CD dimensions, surface functionalization, and core architecture. Bottom-up synthesis using biomass or organic molecular precursors enables heteroatom doping, enhancing quantum efficiency and enabling multicolor emission capabilities. Emerging materials such as TDPC CDs, circularly polarized luminescent CDs, and photochromic afterglow CDs further demonstrate the multifunctional potential of photoresponsive CDs.

These materials exhibit promising applications across diverse fields, including bioimaging, environmental sensing, optoelectronic devices, and dynamic encryption. Due to their low cytotoxicity and tunable emission wavelengths, these materials are ideal fluorescent probes for biological systems. These materials function as sensitive environmental sensors *via* fluorescence quenching mechanisms, enable the fabrication of light-controlled electronic components, and provide innovative encryption solutions through reversible spectral modulation.

Nevertheless, research on photoresponsive CDs faces several challenges, particularly in the nascent field of photochromic variants. Key limitations include the following: (1) underdeveloped systematic design strategies for long-afterglow photoluminescent CDs, with difficulties in regulating emission duration and chromaticity, particularly in organic solvent systems; (2) compromised efficiency and reversibility in solid-state photochromic CDs due to molecular stacking constraints, often requiring auxiliary mechanisms; (3) technical immaturity in synchronizing photochromic transitions with persistent luminescence; (4) challenges in decoupling multiple stimulus-response pathways while maintaining material stability; and (5) complexity in synthetic procedures when integrating photochromic moieties (*e.g.*, NI radicals) with CD matrices. Despite these obstacles, expanding research efforts continue to unveil new applications. As emerging materials with significant potential, photoresponsive CDs are poised to become transformative agents across multiple technological domains.

Data availability

The data that support the findings of this study are available from the corresponding author upon reasonable request.

Conflicts of interest

The authors declare no competing financial interest.

Acknowledgements

We gratefully acknowledge the Youth Talent Program Startup Foundation of Qufu Normal University and Shandong Provincial Natural Science Foundation, projects ZR2024QB412 and ZR2022MB047 supported by Shandong Provincial Natural Science Foundation, and project 602601 supported by Qufu Normal University.

References

1 Y. Niu, F. Wu, Q. Zhang, Y. Teng, Y. Huang, Z. Yang and Z. Mu, *J. Lumin.*, 2024, **275**, 120748.
2 Y. Niu, F. Wu, Y. Zhuo, J. Li, Q. Zhang, Y. Teng, X. Xie, H. Dong and Z. Mu, *Ceram. Int.*, 2025, DOI: **10.1016/j.ceramint.2025.04.252**.
3 X. Xu, R. Ray, Y. Gu, H. J. Ploehn, L. Gearheart, K. Raker and W. A. Scrivens, *J. Am. Chem. Soc.*, 2004, **126**, 12736–12737.
4 H. Liu, X. Zhong, Q. Pan, Y. Zhang, W. Deng, G. Zou, H. Hou and X. Ji, *Coord. Chem. Rev.*, 2024, **498**, 215468.
5 S. Li, L. Li, H. Tu, H. Zhang, D. S. Silvester, C. E. Banks, G. Zou, H. Hou and X. Ji, *Mater. Today*, 2021, **51**, 188–207.
6 Y. Sun, S. Liu, L. Sun, S. Wu, G. Hu, X. Pang, A. T. Smith, C. Hu, S. Zeng, W. Wang, Y. Liu and M. Zheng, *Nat. Commun.*, 2020, **11**, 5591.
7 H. Bai, X. Jin, X. Ma, Y. Zhao, H. Wang, J. Yu, L. Ding, C. Wei, H. Zhou and W. Chen, *Chem. Eng. J.*, 2024, **488**, 150980.
8 S. Yang, H. Zhang, K. Jian, L. Fu, D. Lan and X. Zhao, *Chem. Eng. J.*, 2024, **500**, 157119.
9 M. Jiang, Y. Sun, M. Chen, H. Ji, Y. Liu, R. Qin, X. Li, H. Gao, R. Zhang and L. Zhang, *Chem. Eng. J.*, 2024, **496**, 153761.
10 W. Kasprzyk, P. P. Romańczyk, K. Starzak, A. Wysocka, Ł. Waluda, T. Świergosz, N. V. Bashmakova, G. V. Klishevich, A. M. Dmytruk, I. S. Klyuyev and M. V. Bondar, *Small Struct.*, 2025, **6**, 2400583.
11 P. He, J. Bai, G. Yang, F. Qin, X. Wang, X. Yu, Y. Yao, X. Tang and L. Ren, *Chem. Eng. J.*, 2025, **506**, 160342.
12 M. Cai, Y. Qiu, F. Li, S. Cai and Z. Cai, *ACS Appl. Mater. Interfaces*, 2024, **16**, 46609–46618.
13 Y. Zheng, Q. Zhou, Y. Yang, X. Chen, C. Wang, X. Zheng, L. Gao and C. Yang, *Small*, 2022, **18**, 2201223.
14 J. Sun, Z. Sun, Z. Wang, N. Wang, Y. Han, L. Zhang, B. Zhang and X. Zhang, *Adv. Opt. Mater.*, 2024, **12**, 2302542.
15 Q. Lou, N. Chen, J. Zhu, K. Liu, C. Li, Y. Zhu, W. Xu, X. Chen, Z. Song, C. Liang, C. Shan and J. Hu, *Adv. Mater.*, 2023, **35**, 2211858.
16 X. Hou, J. Xu, P. Zhou, L. Dai, J. Zhang, X. Xiao and K. Huo, *Chem. Eng. J.*, 2023, **478**, 147363.
17 L. He, Z. Li, M. Gu, Y. Li, C. Yi, M. Jiang, X. Yu and L. Xu, *Adv. Sci.*, 2024, **11**, 2406681.
18 J. Ren, K. Ye, H. Opoku, Z. Li, L. Edman and J. Wang, *Carbon*, 2025, **231**, 119706.
19 F. Shan, J. Zhang, C. Liao, Z. Wang and L. Wang, *Chin. Chem. Lett.*, 2023, **34**, 108107.
20 H. A. Nguyen, I. Srivastava, D. Pan and M. Gruebele, *ACS Nano*, 2020, **14**, 6127–6137.
21 L. Ding, X. Jin, Y. Gao, J. Wu, T. Ai, H. Zhou, X. Chen, X. Zhang and W. Chen, *Adv. Opt. Mater.*, 2023, **11**, 2202349.
22 G. Eda, Y. Lin, C. Mattevi, H. Yamaguchi, H. Chen, I. Chen, C. Chen and M. Chhowalla, *Adv. Mater.*, 2010, **22**, 505–509.
23 L. Wang, W. Li, L. Yin, Y. Liu, H. Guo, J. Lai, Y. Han, G. Li, M. Li, J. Zhang, R. Vajtai, P. M. Ajayan and M. Wu, *Sci. Adv.*, 2020, **6**, eabb6772.
24 J. Tan, Q. Li, S. Meng, Y. Li, J. Yang, Y. Ye, Z. Tang, S. Qu and X. Ren, *Adv. Mater.*, 2021, **33**, 2006781.
25 S. Zong, B. Wang, J. Zhang, X. Yu, Y. Zhou, Y. Chen, T. Zhang and J. Li, *Angew. Chem., Int. Ed.*, 2025, **64**, e202420156.
26 X. Han, C. Xia, H. Wu, Y. Xie, R. Li, B. Sui, Y. Yu, B. Wang and B. Yang, *Angew. Chem., Int. Ed.*, 2025, **64**, e202422822.
27 Y. Zhong, Z. Wang, L. Quan, Y. Wu, D. Hu, J. Cheng, Y. Zheng and F. Cheng, *J. Colloid Interface Sci.*, 2025, **679**, 393–402.
28 S. Sun, Q. Fu, Z. Dong and M. Yue, *Chem. Eng. J.*, 2024, **499**, 155972.

29 T. Zhang, M. Wang, L. Liu, Z. Li and H. Bi, *Adv. Funct. Mater.*, 2024, **34**, 2406672.
30 H. Wu, Y. Chen, X. Dai, P. Li, J. F. Stoddart and Y. Liu, *J. Am. Chem. Soc.*, 2019, **141**, 6583–6591.
31 Z. Guo, Y. Bian, L. Zhang, J. Zhang, C. Sun, D. Cui, W. Lv, C. Zheng, W. Huang and R. Chen, *Adv. Mater.*, 2024, **36**, 2409361.
32 Y. Deng, Y. Zhou, S. Ye, J. Qian and S. Cao, *J. Wuhan Univ. Technol., Mater. Sci. Ed.*, 2022, **37**, 23–27.
33 F. Qin, J. Bai, P. He, X. Wang, S. Wu, X. Yu, Y. Yao and L. Ren, *Mater. Today Chem.*, 2023, **34**, 101816.
34 Z. Waseem Basha, S. Muniraj and A. Senthil Kumar, *Sci. Rep.*, 2024, **14**, 9706.
35 L. Cui, X. Ren, J. Wang and M. Sun, *Mater. Today Nano*, 2020, **12**, 100091.
36 S. Yoo, Y. Song and S. Hahn, *Light:Sci. Appl.*, 2022, **11**, 132.
37 S. Karthik, B. Saha, S. K. Ghosh and N. D. Pradeep Singh, *Chem. Commun.*, 2013, **49**, 10471–10474.
38 L. Yan, Z. Cao, L. Ren, T. Zhang, J. Hu, J. Chen, X. Zhang, B. Liu, C. Feng, J. Zhu and B. Geng, *Adv. Healthcare Mater.*, 2024, **13**, 2302190–2302204.
39 Q. Niu, J. Jiang, C. Zhan, Y. Tao, Z. Ye, J. Huang, B. Dong and Z. Kang, *Adv. Funct. Mater.*, 2025, **35**, 2413269–2413276.
40 R. Sinha, N. Roy and T. K. Mandal, *Chem. Eng. J.*, 2022, **431**, 133915–133928.
41 M. Zhou, S. Xu, W. Zhang, G. Shi, Y. He, X. Qiao and X. Pang, *ACS Catal.*, 2024, **14**, 10418–10426.
42 D. Chen, X. Guo, X. Sun, X. Feng, K. Chen, J. Zhang, Z. Zhu, X. Zhang, X. Liu, M. Liu, L. Li and W. Xu, *Exploration*, 2024, **4**, 20230166.
43 Y. Liu, Z. Huang, X. Wang, Y. Hao, J. Yang, H. Wang and S. Qu, *Adv. Funct. Mater.*, 2024, **25**, 2420587.
44 S. Zhu, Y. Song, J. Shao, X. Zhao and B. Yang, *Angew. Chem., Int. Ed.*, 2015, **54**, 14626–14637.
45 Y. Jiang, T. Zhao, W. Xu and Z. Peng, *Carbon*, 2024, **219**, 118838.
46 J. E. Abraham, P. Kumbhakar and M. Balachandran, *J. Fluoresc.*, 2025, **35**, 2049–2058.
47 J. E. Abraham and M. Balachandran, *J. Fluoresc.*, 2022, **32**, 887–906.
48 L. Ai, W. Xiang, J. Xiao, H. Liu, J. Yu, L. Zhang, X. Wu, X. Qu and S. Lu, *Adv. Mater.*, 2024, **36**, 2401220.
49 R. Chen, Y. Guan, H. Wang, Y. Zhu, X. Tan, P. Wang, X. Wang, X. Fan and H.-L. Xie, *ACS Appl. Mater. Interfaces*, 2021, **13**, 41131–41139.
50 L. Jiang, H. Ding, S. Lu, T. Geng, G. Xiao, B. Zou and H. Bi, *Angew. Chem., Int. Ed.*, 2020, **59**, 9986–9991.
51 S. Helmy, F. A. Leibfarth, S. Oh, J. E. Poelma, C. J. Hawker and J. Read De Alaniz, *J. Am. Chem. Soc.*, 2014, **136**, 8169–8172.
52 A. T. Mogharbel, A. Hameed, A. A. Sayqal, H. A. Katouah, S. D. Al-Qahtani, F. A. Saad and N. M. El-Metwaly, *Int. J. Biol. Macromol.*, 2023, **238**, 124028.
53 Y. Yan, Y. Wu, Q. Wang, Y. Wang, Y. Zhan, Z. Sun, L. Yu and X. Wang, *Adv. Opt. Mater.*, 2023, **11**, 2203019.
54 K. Jin, X. Ji, T. Yang, J. Zhang, W. Tian, J. Yu, X. Zhang, Z. Chen and J. Zhang, *Chem. Eng. J.*, 2021, **406**, 126794.
55 S. D. Al-Qahtani, A. Hameed, R. M. Snari, R. Shah, A. Abdulaziz Alfi, F. Shaaban and N. M. El-Metwaly, *J. Mol. Liq.*, 2022, **354**, 118927.
56 J. Wu, S. Fu, X. Zhang, C. Wu, A. Wang, C. Li, G. Shan and Y. Liu, *ACS Appl. Mater. Interfaces*, 2020, **12**, 6262–6267.
57 Z. Yan, J. Shu, Y. Yu, Z. Zhang, Z. Liu and J. Chen, *Luminescence*, 2015, **30**, 388–392.
58 L. Tian, D. Ghosh, W. Chen, S. Pradhan, X. Chang and S. Chen, *Chem. Mater.*, 2009, **21**, 2803–2809.
59 L. Đorđević, F. Arcudi, M. Cacioppo and M. Prato, *Nat. Nanotechnol.*, 2022, **17**, 112–130.
60 J. Li, C. Sun, Q. Li, X. Xu, B. Li, Y. Tian, D. Zheng, R. Yao, K. Yuan and Z. Guo, *ChemSusChem*, 2025, **18**, e202401313.
61 P.-C. Hsu and H.-T. Chang, *Chem. Commun.*, 2012, **48**, 3984.
62 S.-L. Hu, K.-Y. Niu, J. Sun, J. Yang, N.-Q. Zhao and X.-W. Du, *J. Mater. Chem.*, 2009, **19**, 484–488.
63 L. Cai, Y. Wang, D. Xu, H. Chen and Y. Zhao, *Chem. Eng. J.*, 2023, **461**, 142000.
64 L. Hernández-Tabares, J. G. Darias-González, J. Artechе-Díaz, E. Carrillo-Barroso, L. M. Ledo-Pereda and L. F. Desdín-García, *Adv. Nat. Sci.: Nanosci. Nanotechnol.*, 2018, **9**, 35002.
65 F. J. Chao-Mujica, L. Garcia-Hernández, S. Camacho-López, M. Camacho-López, M. A. Camacho-López, D. Reyes Contreras, A. Pérez-Rodríguez, J. P. Peña-Caravaca, A. Páez-Rodríguez, J. G. Darias-Gonzalez, L. Hernandez-Tabares, O. Arias De Fuentes, E. Prokhorov, N. Torres-Figueredo, E. Reguera and L. F. Desdin-García, *J. Appl. Phys.*, 2021, **129**, 163301.
66 Y.-P. Sun, B. Zhou, Y. Lin, W. Wang, K. A. S. Fernando, P. Pathak, M. J. Meziani, B. A. Harruff, X. Wang, H. Wang, P. G. Luo, H. Yang, M. E. Kose, B. Chen, L. M. Veca and S.-Y. Xie, *J. Am. Chem. Soc.*, 2006, **128**, 7756–7757.
67 H. Peng and J. Travas-Sejdic, *Chem. Mater.*, 2009, **21**, 5563–5565.
68 Y. Dong, N. Zhou, X. Lin, J. Lin, Y. Chi and G. Chen, *Chem. Mater.*, 2010, **22**, 5895–5899.
69 J. Zhou, C. Booker, R. Li, X. Zhou, T.-K. Sham, X. Sun and Z. Ding, *J. Am. Chem. Soc.*, 2007, **129**, 744–745.
70 Y. Yuan, X. Bao, L. Wu, M. Zhou, Y. Yu, Q. Wang and P. Wang, *Chem. Eng. J.*, 2024, **493**, 152488.
71 W. Wang, J. Wu, Y. Xing and Z. Wang, *Sens. Actuators, B*, 2022, **360**, 131645.
72 H. Ding, J. Wei, P. Zhang, Z. Zhou, Q. Gao and H. Xiong, *Small*, 2018, **14**, 1800612.
73 Y. Liu, J. H. Lei, G. Wang, Z. Zhang, J. Wu, B. Zhang, H. Zhang, E. Liu, L. Wang, T. Liu, G. Xing, D. Ouyang, C. Deng, Z. Tang and S. Qu, *Adv. Sci.*, 2022, **9**, 2202283.
74 Z. Sun, F. Yan, J. Xu, H. Zhang and L. Chen, *Nano Res.*, 2022, **15**, 414–422.
75 Z. Tian, X. Zhang, D. Li, D. Zhou, P. Jing, D. Shen, S. Qu, R. Zboril and A. L. Rogach, *Adv. Opt. Mater.*, 2017, **5**, 1700416.
76 H. Lu, S. Xu and J. Liu, *ACS Sens.*, 2019, **4**, 1917–1924.
77 J. Liao, M. Wu, J. Li and X. Gong, *Adv. Opt. Mater.*, 2025, **13**, 2402472.

78 J. Cao, R. Chen, L. Wang, H. Xing, H. Hu, X. Yang, C. Gu, S. Tang and D. Chen, *Chem. Eng. J.*, 2024, **491**, 152121.
79 Z. Yao, X. Wen, X. Hong, R. Tao, F. Yin, S. Cao, J. Yan, K. Wang and J. Wang, *Adv. Sci.*, 2024, **11**, 2308523.
80 R. Li, S. Tao, J. Liu, X. Han, C. Xia and B. Yang, *Small Struct.*, 2024, **07**, 2400447.
81 S. Zhu, Q. Meng, L. Wang, J. Zhang, Y. Song, H. Jin, K. Zhang, H. Sun, H. Wang and B. Yang, *Angew. Chem., Int. Ed.*, 2013, **52**, 3953–3957.
82 F. Cui, J. Sun, J. De Dieu Habimana, X. Yang, J. Ji, Y. Zhang, H. Lei, Z. Li, J. Zheng, M. Fan and X. Sun, *Anal. Chem.*, 2019, **91**, 14681–14690.
83 C. Wei, S. Hu, F. Liang, Z. Song and X. Liu, *Chin. Chem. Lett.*, 2022, **33**, 4116–4120.
84 J. Wen, Z. Zeng, B. Wang, J. Hong, Y. Chen, J. Zhang, J. Li and J. Jiang, *Nano Res.*, 2023, **16**, 7761–7769.
85 K. Jiang, Y. Wang, X. Gao, C. Cai and H. Lin, *Angew. Chem., Int. Ed.*, 2018, **57**, 6216–6220.
86 Z. Luo, G. Qi, K. Chen, M. Zou, L. Yuwen, X. Zhang, W. Huang and L. Wang, *Adv. Funct. Mater.*, 2016, **26**, 2739–2744.
87 J.-N. Hao, Z.-Z. Ding, C.-L. Shen, G.-S. Zheng, J.-L. Liu, R.-B. Li, R.-W. Song, K.-K. Liu, J.-H. Zang, L. Dong, Q. Lou and C.-X. Shan, *Chem. Eng. J.*, 2024, **486**, 150196.
88 Z. Wan, Y. Li, Y. Zhou, D. Peng, X. Zhang, J. Zhuang, B. Lei, Y. Liu and C. Hu, *Adv. Funct. Mater.*, 2023, **33**, 2207296.
89 H. Ding, R. Zhao, Z.-H. Zhang, J.-J. Yang, Z. Wang, L.-L. Xiao, X.-H. Li, X.-J. He and H.-M. Xiong, *Chem. Eng. J.*, 2023, **476**, 146405.
90 G. Hu, Y. Wang, S. Zhang, H. Ding, Z. Zhou, J. Wei, X. Li and H. Xiong, *Carbon*, 2023, **203**, 1–10.
91 Y. Su, Z. Xie and M. Zheng, *J. Colloid Interface Sci.*, 2020, **573**, 241–249.
92 C. Russo, A. Carpentieri, A. Tregrossi, A. Ciajolo and B. Apicella, *Carbon*, 2023, **201**, 900–909.
93 A. B. Bourlinos, A. Stassinopoulos, D. Anglos, R. Zboril, M. Karakassides and E. P. Giannelis, *Small*, 2008, **4**, 455–458.
94 H. Hu, J. Li and X. Gong, *Small*, 2024, **20**, 2308457.
95 Y. Li, C. Liu, H. Sun, M. Chen, D. Hou, Y. Zheng, H. Xie, B. Zhou and X. Lin, *Adv. Sci.*, 2023, **10**, 2300543.
96 X. Miao, D. Qu, D. Yang, B. Nie, Y. Zhao, H. Fan and Z. Sun, *Adv. Mater.*, 2018, **30**, 1704740.
97 X. Gao, K. Pan, B. Zhao and J. Deng, *Adv. Funct. Mater.*, 2025, **35**, 2413569.
98 K. Luo, W. Li, X. Luo, X. Kang and Y. Wen, *Diamond Relat. Mater.*, 2024, **142**, 110837.
99 H. Sun, P. Xia, H. Shao, R. Zhang, C. Lu, S. Xu and C. Wang, *J. Colloid Interface Sci.*, 2023, **646**, 932–939.
100 X. Wang, Q. Zhao, Q. Song, H. Bu, J. Gao, L. Li, X. Yu, X. Yang, Z. Lu and X. Zhang, *Spectrochim. Acta, Part A*, 2024, **310**, 123952.
101 Y. Yan, J. H. Liu, R. S. Li, Y. F. Li, C. Z. Huang and S. J. Zhen, *Anal. Chim. Acta*, 2019, **1063**, 144–151.
102 M.-C. Rong, K.-X. Zhang, Y.-R. Wang and X. Chen, *Chin. Chem. Lett.*, 2017, **28**, 1119–1124.
103 G. Xu, J. Shen, L. Zhang, L. Lin, X. Zheng, X. Xu, P. Du and H. Xu, *Colloids Surf., A*, 2024, **687**, 133486.
104 Z. Huo, L. Xia, G. Li and X. Xiao, *Chem. – Eur. J.*, 2020, **26**, 14754–14764.
105 S. Zhang, L. Zhang, L. Huang, G. Zheng, P. Zhang, Y. Jin, Z. Jiao and X. Sun, *J. Lumin.*, 2019, **206**, 608–612.
106 G. Raniszewski, M. Pyc and Z. Kolacinski, *Sensors*, 2014, **14**, 18474–18483.
107 X. Li, H. Wang, Y. Shimizu, A. Pyatenko, K. Kawaguchi and N. Koshizaki, *Chem. Commun.*, 2011, **47**, 932–934.
108 A. I. Sidorov, V. F. Lebedev, A. A. Kobranova and A. V. Nashchekin, *Quantum Electron.*, 2018, **48**, 45–48.
109 Y. Song, C. Zhu, J. Song, H. Li, D. Du and Y. Lin, *ACS Appl. Mater. Interfaces*, 2017, **9**, 7399–7405.
110 Z.-A. Qiao, Y. Wang, Y. Gao, H. Li, T. Dai, Y. Liu and Q. Huo, *Chem. Commun.*, 2010, **46**, 8812.
111 J. Gao, X. Wu, X. Jiang, M. Li, R. He and W. Shen, *Carbon*, 2023, **208**, 365–373.
112 D. Yang, T. Shao, L. Zhang, X. Wang and Q. Yue, *Food Chem.*, 2025, **472**, 142905.
113 X. Bian, X. Lu, Y. Huang, X. Wen and Z. Fan, *Sens. Actuators, B*, 2025, **428**, 137265.
114 X. Gong, Y. Wu, J. Li, S. Zhang and M. Wu, *Carbon*, 2024, **226**, 119208.
115 C. Wu, S. Zhang, M. Liu and J. He, *Carbon*, 2024, **230**, 119601.
116 X. Guo, R. Yang, Y. Wang, C. Cheng, D. Fu and J. Sheng, *Int. J. Biol. Macromol.*, 2023, **253**, 126723.
117 Y. Liu, N. Xiao, N. Gong, H. Wang, X. Shi, W. Gu and L. Ye, *Carbon*, 2014, **68**, 258–264.
118 D. Li, C. Liang, E. V. Ushakova, M. Sun, X. Huang, X. Zhang, P. Jing, S. J. Yoo, J. Kim, E. Liu, W. Zhang, L. Jing, G. Xing, W. Zheng, Z. Tang, S. Qu and A. L. Rogach, *Small*, 2019, **15**, 1905050.
119 L. Stan, I. Volf, C. S. Stan, C. Albu, A. Coroaba, L. E. Ursu and M. Popa, *Nanomaterials*, 2022, **13**, 131.
120 S. Chernyak, A. Podgornova, S. Dorofeev, S. Maksimov, K. Maslakov, S. Savilov and V. Lunin, *Appl. Surf. Sci.*, 2020, **507**, 145027.
121 R. Liu, D. Wu, S. Liu, K. Koynov, W. Knoll and Q. Li, *Angew. Chem., Int. Ed.*, 2009, **48**, 4598–4601.
122 M. Gagana, B. R. Radha Krushna, S. C. Sharma, R. Reeta, S. Mishra, B. Sargunam, P. Josson Akkara, K. Suresh Babu and H. Nagabhushana, *Inorg. Chem. Commun.*, 2024, **170**, 113468.
123 W. Zhong and J. Yang, *Sci. Total Environ.*, 2024, **957**, 177473.
124 F. Lu, X. Xu, W. Wan, X. Liang, J. Xia, W. Cao, Z. Chen and M. Hu, *J. Mater. Chem. C*, 2025, **13**, 2091–2120.
125 L. Cao, M. Zan, F. Chen, X. Kou, Y. Liu, P. Wang, Q. Mei, Z. Hou, W.-F. Dong and L. Li, *Carbon*, 2022, **194**, 42–51.
126 S. Zhu, Y. Song, J. Wang, H. Wan, Y. Zhang, Y. Ning and B. Yang, *Nano Today*, 2017, **13**, 10–14.
127 H. Li, X. He, Z. Kang, H. Huang, Y. Liu, J. Liu, S. Lian, C. H. A. Tsang, X. Yang and S. Lee, *Angew. Chem., Int. Ed.*, 2010, **49**, 4430–4434.
128 M. Cao, X. Zhao and X. Gong, *Small*, 2022, **18**, 2106683.
129 H. Guo, Y. Lu, Z. Lei, H. Bao, M. Zhang, Z. Wang, C. Guan, B. Tang, Z. Liu and L. Wang, *Nat. Commun.*, 2024, **15**, 4843.

130 F. Yuan, Z. Wang, X. Li, Y. Li, Z. Tan, L. Fan and S. Yang, *Adv. Mater.*, 2017, **29**, 1604436.
131 Z. Liu, H. Zou, N. Wang, T. Yang, Z. Peng, J. Wang, N. Li and C. Huang, *Sci. China:Chem.*, 2018, **61**, 490–496.
132 C. Huang, M. Feng, X. Zhu, Q. Zhou, S. Zeng, Y. Huang and H. Zhang, *Macromolecules*, 2021, **54**, 11497–11507.
133 P. Li, S. Xue, L. Sun, X. Ma, W. Liu, L. An, Y. Liu, D. Qu and Z. Sun, *Small*, 2024, **20**, 2310563.
134 Y. Li, C. Lei, J. Yang, X. Liu and K. Zhang, *Appl. Surf. Sci.*, 2022, **606**, 154939.
135 Y. Zhang, S. Ding, J. Yu, L. Sui, H. Song, Y. Hu, G. I. N. Waterhouse, Z. Tang and S. Lu, *Matter*, 2024, **7**, 3518–3536.
136 Y. Song, S. Zhu, S. Zhang, Y. Fu, L. Wang, X. Zhao and B. Yang, *J. Mater. Chem. C*, 2015, **3**, 5976–5984.
137 X. Yao, Y. Wang, F. Li, J. J. Dalluge, G. Orr, R. Hernandez, Q. Cui and C. L. Haynes, *Nanoscale*, 2022, **14**, 9516–9525.
138 C. Xia, S. Zhu, S.-T. Zhang, Q. Zeng, S. Tao, X. Tian, Y. Li and B. Yang, *ACS Appl. Mater. Interfaces*, 2020, **12**, 38593–38601.
139 S. Zhu, J. Zhang, S. Tang, C. Qiao, L. Wang, H. Wang, X. Liu, B. Li, Y. Li, W. Yu, X. Wang, H. Sun and B. Yang, *Adv. Funct. Mater.*, 2012, **22**, 4732–4740.
140 Y. Zhou, E. M. Zahran, B. A. Quiroga, J. Perez, K. J. Mintz, Z. Peng, P. Y. Liyanage, R. R. Pandey, C. C. Chusuei and R. M. Leblanc, *Appl. Catal. B: Environ.*, 2019, **248**, 157–166.
141 J. Zhu, H. Shao, X. Bai, Y. Zhai, Y. Zhu, X. Chen, G. Pan, B. Dong, L. Xu, H. Zhang and H. Song, *Nanotechnology*, 2018, **29**, 245702.
142 T. Li, W. Shi, E. Shuang, Q. Mao and X. Chen, *J. Colloid Interface Sci.*, 2021, **591**, 334–342.
143 B. Zhang, B. Wang, E. V. Ushakova, B. He, G. Xing, Z. Tang, A. L. Rogach and S. Qu, *Small*, 2023, **19**, 2204158.
144 Z. Song, Y. Liu, X. Lin, Z. Zhou, X. Zhang, J. Zhuang, B. Lei and C. Hu, *ACS Appl. Mater. Interfaces*, 2021, **13**, 34705–34713.
145 H. Shi, Y. Wu, J. Xu, C. Zhou, H. Xu, W. Ye, Y. Yin, Z. Wang, R. Su, Z. An and H. Shi, *Chem. Eng. J.*, 2023, **476**, 146524.
146 B. Wang, Z. Sun, J. Yu, G. I. N. Waterhouse, S. Lu and B. Yang, *SmartMat*, 2022, **3**, 337–348.
147 S. Zhu, L. Wang, N. Zhou, X. Zhao, Y. Song, S. Maharjan, J. Zhang, L. Lu, H. Wang and B. Yang, *Chem. Commun.*, 2014, **50**, 13845–13848.
148 S. Lu, L. Sui, J. Liu, S. Zhu, A. Chen, M. Jin and B. Yang, *Adv. Mater.*, 2017, **29**, 1603443.
149 S. Tao, C. Zhou, C. Kang, S. Zhu, T. Feng, S.-T. Zhang, Z. Ding, C. Zheng, C. Xia and B. Yang, *Light: Sci. Appl.*, 2022, **11**, 56.
150 C. Xia, J. Zhong, X. Han, S. Zhu, Y. Li, H. Liu and B. Yang, *Angew. Chem., Int. Ed.*, 2024, **63**, e202410519.
151 C. Zheng, S. Tao, X. Zhao, C. Kang and B. Yang, *Angew. Chem., Int. Ed.*, 2024, **63**, e202408516.
152 K. Zhang, Q. Fu, S. Sun, Z. Dong and M. Yue, *ACS Appl. Mater. Interfaces*, 2024, **16**, 52833–52841.
153 X. Ma, S. Liuye, K. Ning, X. Wang, S. Cui and S. Pu, *Photochem. Photobiol. Sci.*, 2023, **22**, 2389–2399.
154 X. Wang, S. Liuye, X. Ma, S. Cui and S. Pu, *Dyes Pigm.*, 2023, **216**, 111318.
155 J. Zhu, H. Zhao, Y. Yang, W. Wu, L. Hu, Y. Wei and Y. Gao, *Sci. China Mater.*, 2024, **67**, 680–689.
156 J. Zhu, Y. Yang, J. He, L. Hu, W. Wu, Y. Gao and Y. Wei, *ACS Appl. Opt. Mater.*, 2023, **1**, 1312–1319.
157 J. Wan, J. Xu, S. Zhu, J. Li and K. Chen, *Sustainable Mater. Technol.*, 2024, **40**, e00866.
158 Y. Sun, D. Zhang, G. Ren, S. Zhou, L. Tian and L. Zhou, *Chem. Phys. Lett.*, 2024, **840**, 141114–141121.
159 W. Gao, S. Xiang, M. Bai, Y. Ruan, J. Zheng, X. Cao, Y. Xu, Y. Chen and W. Weng, *Polymer*, 2022, **257**, 125278.
160 M. Razaghi, M. Khorasani, Z. Mohamadnia and F. Kazemi, *J. Photochem. Photobiol., A*, 2023, **437**, 114420.
161 A. Wang, X. Xiao, C. Zhou, F. Lyu, L. Fu, C. Wang and S. Ruan, *Nanoscale Adv.*, 2019, **1**, 1819–1825.
162 M. Deng, Y. Zhang, Y. Wang and S. Jiang, *J. Mater. Chem. C*, 2020, **8**, 15697–15704.
163 L. Ai, H. Liu, R. Liu, H. Song, Z. Song, M. Nie, G. I. N. Waterhouse and S. Lu, *Sci. China:Chem.*, 2022, **65**, 2274–2282.
164 Y. Liu, M. Al-salihi, Y. Guo, R. Ziniuk, S. Cai, L. Wang, Y. Li, Z. Yang, D. Peng, K. Xi, Z. An, X. Jia, L. Liu, W. Yan and J. Qu, *Light:Sci. Appl.*, 2022, **11**, 163.
165 Y. Wen, Q. Jia, F. Nan, X. Zheng, W. Liu, J. Wu, H. Ren, J. Ge and P. Wang, *Chem. – Asian J.*, 2019, **14**, 2162–2168.
166 X. Wu, M. Xu, S. Wang, K. Abbas, X. Huang, R. Zhang, A. C. Tedesco and H. Bi, *Dalton Trans.*, 2022, **51**, 2296–2303.
167 G. Jiang, J. Fan, Y. Wan, J. Li and F. Pi, *Chem. Eng. J.*, 2024, **480**, 148216–148224.
168 C. H. Lee, S. Y. Song, Y. J. Chung, E. K. Choi, J. Jang, D. H. Lee, H. D. Kim, D.-U. Kim and C. B. Park, *ACS Appl. Bio Mater.*, 2022, **5**, 761–770.
169 Y. Xu, H. Yu, L. Chudal, N. K. Pandey, E. H. Amador, B. Bui, L. Wang, X. Ma, S. Deng, X. Zhu, S. Wang and W. Chen, *Mater. Today Phys.*, 2021, **17**, 100328–100342.
170 X. Zhang, X. Tan and Y. Hu, *J. Hazard. Mater.*, 2021, **411**, 125184–125191.
171 Z. Jia, Y. Liu, L. Cheng, Z. Deng, M. Zhang and H. Tuo, *Front. Chem.*, 2023, **11**, 1288418.
172 H. Yang, M. Xia, W. Yang, H. Liu, P. Ni and Y. Lu, *Sens. Actuators, B*, 2025, **428**, 137231–137240.
173 R. Yuan, B. Yan, C. Lai, X. Wang, Y. Cao, J. Tu, Y. Li and Q. Wu, *ACS Omega*, 2023, **8**, 22099–22107.
174 X.-C. Yang, Y.-L. Yang, S.-L. Zhang, Y.-F. Liu, S.-J. Fu, M. Zhu, J.-F. Hu, Z.-J. Zhang and J.-T. Zhao, *Appl. Surf. Sci.*, 2019, **490**, 592–597.
175 Z. Tian, D. Li, E. V. Ushakova, V. G. Maslov, D. Zhou, P. Jing, D. Shen, S. Qu and A. L. Rogach, *Adv. Sci.*, 2018, **5**, 1800795.
176 F. Liu, Z. Li, Y. Li, Y. Feng and W. Feng, *Carbon*, 2021, **181**, 9–15.
177 Q. Li, D. Cheng, H. Gu, D. Yang, Y. Li, S. Meng, Y. Zhao, Z. Tang, Y. Zhang, J. Tan and S. Qu, *Chem. Eng. J.*, 2023, **462**, 142339.
178 Z. Han, P. Li, Y. Deng and H. Li, *Chem. Eng. J.*, 2021, **415**, 128999.
179 H. Zhang, X. Guo, K. Jian, L. Fu and X. Zhao, *Inorg. Chem.*, 2023, **62**, 13847–13856.

180 S. Hu, W. Yang, N. Li, H. Wang, J. Yang and Q. Chang, *Small*, 2018, **14**, 1803447–1803455.
181 M. Zhang, Y. Zhang, X. Du, Y. Ma, H. Huang, F. Liao, X. Fan, J. Wang, H. Lin, M. Shao, Y. Liu, Y. Li and Z. Kang, *ACS Appl. Mater. Interfaces*, 2024, **16**, 19379–19390.
182 T. Fatima, S. Husain and M. Khanuja, *Nano Mater. Sci.*, 2024, S2589965124000485.
183 G. Filippini, F. Amato, C. Rosso, G. Ragazzon, A. Vega-Peñaloza, X. Companyó, L. Dell'Amico, M. Bonchio and M. Prato, *Chem*, 2020, **6**, 3022–3037.
184 J.-F. Li, C.-Y. Zhong, J.-R. Huang, Y. Chen, Z. Wang and Z.-Q. Liu, *J. Colloid Interface Sci.*, 2019, **553**, 758–767.
185 H. Wu, S. Lu and B. Yang, *Acc. Mater. Res.*, 2022, **3**, 319–330.
186 W. Dong, X. Zhang, F. Yang, Q. Zeng, W. Yin, W. Zhang, H. Wang, X. Yang, S. V. Kershaw, B. Yang, A. L. Rogach and W. Zheng, *ACS Nano*, 2022, **16**, 9679–9690.
187 B. Zhao and Z. Tan, *Adv. Sci.*, 2021, **8**, 2001977.
188 C. Kütahya, P. Wang, S. Li, S. Liu, J. Li, Z. Chen and B. Strehmel, *Angew. Chem., Int. Ed.*, 2020, **59**, 3166–3171.
189 J. Shen, T. Zhang, J. Li, Z. Li, H. Yu, W. Yuan, H. Huang, Y. Liu and Z. Kang, *Adv. Funct. Mater.*, 2024, **34**, 2408239.
190 C. Ji, Q. Han, Y. Zhou, J. Wu, W. Shi, L. Gao, R. M. Leblanc and Z. Peng, *Carbon*, 2022, **192**, 198–208.
191 R. Chen, Z. Wang, T. Pang, Q. Teng, C. Li, N. Jiang, S. Zheng, R. Zhang, Y. Zheng, D. Chen and F. Yuan, *Adv. Mater.*, 2023, **35**, 2302275.
192 B. Xu, J. Li, J. Zhang, H. Ning, X. Fang, J. Shen, H. Zhou, T. Jiang, Z. Gao, X. Meng and Z. Wang, *Adv. Sci.*, 2023, **10**, 2205788–2205796.
193 W. Sun, Y. Zhang, G. Yin and S. Lu, *Adv. Funct. Mater.*, 2024, **34**, 2402346–2402354.
194 Z. Wang, N. Jiang, M. Liu, R. Zhang, F. Huang and D. Chen, *Small*, 2021, **17**, 2104551.
195 B. Zhao, H. Ma, H. Jia, M. Zheng, K. Xu, R. Yu, S. Qu and Z. Tan, *Angew. Chem., Int. Ed.*, 2023, **62**, e202301651-NaN.
196 S. Xiong, C. Yan and Y. Qi, *Nano Mater. Sci.*, 2024, S2589965124000886.
197 S. Paul, S. Hazra and A. Banerjee, *ACS Sustainable Chem. Eng.*, 2021, **9**, 12912–12921.
198 N. Prishkolnik, N. Shauloff, S. Kanti Bhaumik, S. Biswas, A. Morag and R. Jelinek, *Small Struct.*, 2025, **6**, 2400533–2400543.
199 X. Liu, L. Sun, F. Zhai, T. Wu, P. Wang, H. Du, Y. Xu and X. Wang, *Adv. Energy Mater.*, 2025, 202405433.
200 A. Abbas, C. Zhang, S. Hussain, Y. Li, R. Gao, J. Li, X. Liu, M. Zhang and S. Xu, *Small*, 2023, **19**, 2206621–2206631.
201 S. Wu, W. Li, Y. Sun, X. Pang, X. Zhang, J. Zhuang, H. Zhang, C. Hu, B. Lei and Y. Liu, *J. Mater. Chem. C*, 2020, **8**, 8935–8941.
202 Y. Wu, L. Zeng, Y. Zheng, F. You and X. Liu, *Appl. Surf. Sci.*, 2025, **687**, 162245–162259.
203 A. Ponnusamy, A. Khan, T. Prodpran, J. T. Kim, S. Benjakul and J.-W. Rhim, *Int. J. Biol. Macromol.*, 2025, **288**, 138692–138703.
204 Z. Riahi, A. Khan, J.-W. Rhim, G. H. Shin and J. T. Kim, *Sustainable Mater. Technol.*, 2025, **43**, e01217-NaN.
205 L. Mao, Z. Dong, F. Dong, X. Dai and Z. Cao, *Int. J. Biol. Macromol.*, 2025, **296**, 139738–139748.